Ultrafast Materials Synthesis and Manufacturing Techniques for Emerging Energy and Environmental Applications

AUTHOR(S): Xueshan Hu[1,#], Daxian Zuo[1,#], Shaoru Cheng[1,#], Sihui Chen[1], Yang Liu[1], Wenzhong Bao[2], Sili Deng[3], Stephen J. Harris[4], Jiayu Wan[1,*]

ADDRESS:
[1]Department of Mechanical and Energy Engineering, Southern University of Science and Technology, Shenzhen, China, 518055
[2]State Key Laboratory of ASIC and System, School of Microelectronics, Fudan University, Shanghai, China, 200433
[3]Department of Mechanical Engineering, Massachusetts Institute of Technology, Cambridge, MA, USA 02139
[4]Energy Storage Division, Lawrence Berkeley National Laboratory, Berkeley, CA, USA, 94720
EMAIL: wanjy@sustech.edu.cn

Abstract

Energy and environmental issues have attracted increasing attention globally, where sustainability and low-carbon emissions are seriously considered and widely accepted by government officials. In response to this situation, the development of renewable energy and environmental technologies is urgently needed to complement the usage of traditional fossil fuels. While a big part of advancement in these technologies relies on materials innovations, new materials discovery is limited by sluggish conventional materials synthesis methods, greatly hindering the advancement of related technologies. To address this issue, this review introduces and comprehensively summarizes emerging ultrafast materials synthesis methods that could synthesize materials in times as short as nanoseconds, significantly improving research efficiency. We discuss the unique advantages of these methods, followed by how they benefit individual applications for renewable energy and the environment. We also highlight the scalability of ultrafast manufacturing towards their potential industrial utilization. Finally, we provide our perspectives on challenges and opportunities for the future development of ultrafast synthesis and manufacturing technologies. We anticipate that fertile opportunities exist not only for energy and the environment but also for many other applications.

1. Introduction

The industrial revolutions in the past few centuries have fundamentally changed our way of energy utilization, bringing significant advances in human society. However, the development of modern society relies on a large amount of energy consumption, which is mainly supplied by fossil fuels. The continuous consumption of resources leads to the emission of significant amounts of greenhouse gases, resulting in the increasingly harmful effect of global warming, endangering the balance of natural ecosystems and the human living environment. To address this concern, countries

worldwide have introduced related policies.[1-4] For example, (a) The United States passed the Clean Energy and Security Act and released the National Blueprint for Lithium Battery 2021-2030.[5,6] (b) Europe: deployed the EU Horizon 2020 Plan that embraces a low-carbon future.[7-10] (c) Japan proposed the Carbon-neutral and Green Growth Strategy in 2050, focusing on promoting the development of green industries.[11-17] (d) China is actively promoting green and low-carbon development and promises to achieve Carbon Peaks by 2030 and Carbon Neutrality by 2060.[18-21] In short, it is widely accepted that developing renewable energy and environmental technologies has become a pressing task for humanity.
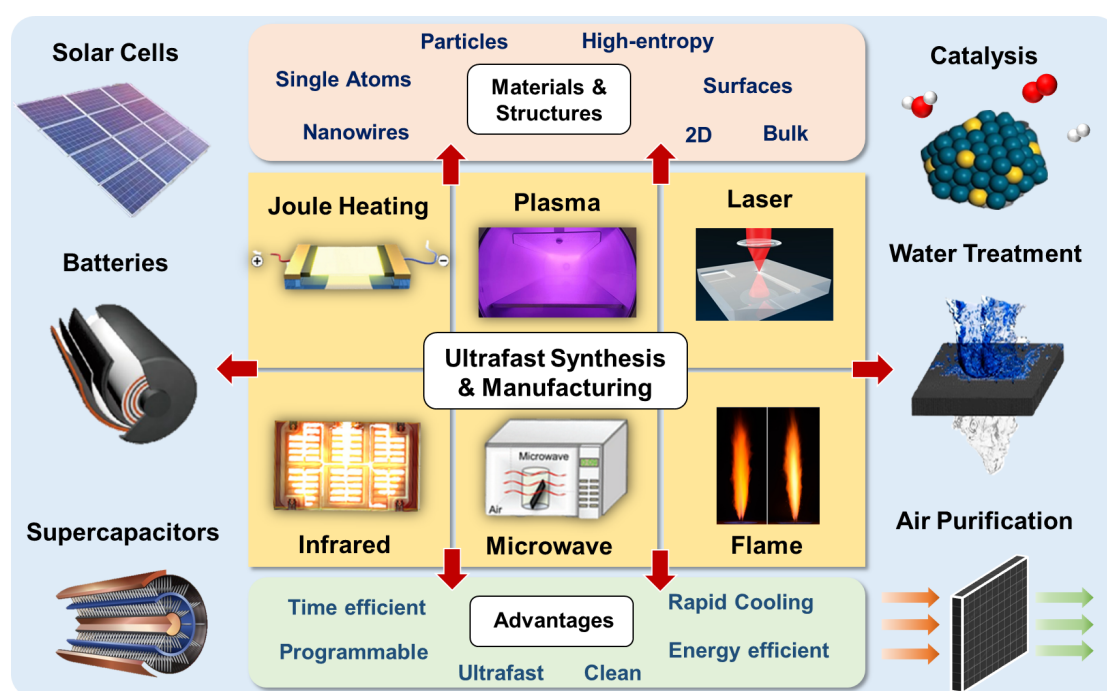

Fig. 1 Summary of ultrafast synthesis & manufacturing methods and related applications. Reproduced with permission.[22] Copyright 2016, American Chemical Society. Reproduced with permission.[23] Copyright 2017, American Chemical Society. Reproduced with permission[24] Reproduced with permission[25] Copyright 2014, John Wiley & Sons, Inc. Reproduced with permission.[26] Copyright 2020, Elsevier Ltd. Reproduced with permission.[27] Copyright 2019, John Wiley & Sons, Inc. Reproduced with permission.[28] Copyright 2019, AIP Publishing Inc. Reproduced with permission.[29] Copyright 2017, Elsevier Ltd. Reproduced with permission.[30] Copyright 2010, American Chemical Society.

In response, academia and industry are working hard to develop sustainable technologies for energy and the environment. The development of these technologies is inseparable from the development and application of new materials. However, preparing new materials via most conventional methods, such as the hydrothermal method or the furnace-assisted calcination method is still inefficient. This is because they usually operate at high temperature, requiring hours or even days to obtain even one batch of sample, consuming much energy and time. Plus, these methods are often labor-intensive, further reducing research efficiency. To overcome this time-limiting

hurdle and accelerate the R&D of new energy and environmental technologies, novel material preparation and manufacturing methods that can substantially reduce time, labor, and energy consumption are urgently needed.

This review article provides an overview of emerging ultrafast materials synthesis technologies for energy and environmental applications to address the above concerns. Representative ultrafast manufacturing methods include laser-assisted synthesis, microwave-assisted synthesis, joule heating, infrared synthesis, plasma synthesis, and flame-assisted synthesis etc (**Fig. 1**). These methods rely on the immediate release of energy, which provides instantaneous high power/temperature for materials synthesis. The unique advantages of the emerging ultrafast manufacturing methods include:

1) **These methods are ultrafast and highly efficient**.[31-35] Unlike conventional methods that take hours or even days, ultrafast synthesis methods usually require a few nanoseconds to a few minutes. The short reaction times of ultrafast methods not only provide a more precise and targeted energy input, but also can considerably reduce the unavoidable heat dissipation through radiation, convection, and conduction. Plus, these methods generally involve significantly fewer synthesis steps than conventional methods, such as the time-consuming furnace/oven heating and the inefficient solvent-intensive washing. Thus, the short reaction time leads to superior energy utilization and efficiency compared to traditional methods.

2) **These methods can synthesize materials that are nearly inaccessible to conventional methods**.[36-38] A common characteristic of ultrafast synthesis methods is that they generally utilize instantaneously-released energy, reaching temperatures as high as 3000 K, which triggers the desired reactions for materials synthesis. As a result, kinetically unfavorable reactions that are not possible at normal conditions (e.g. furnace heating and cooling under normal pressure) may become favorable using ultrafast synthesis techniques. Furthermore, compared with conventional thermal approaches that require hours at high temperatures, the ultrafast characteristic of these methods allows the synthesis of materials that require temperature-sensitive substrates/supports (as they might only need to get exposed at high energy/temperature in seconds).

3) **Synthesized materials with ultrafast methods can remain in their metastable state**.[39-42] The heating and cooling processes of these methods are typically short, providing little time for long-range diffusion within as-synthesized materials. After cool-down, kinetic barriers may prevent atomistic diffusion and lead to stabilization of the products. Thus, as-synthesized materials can easily stay in metastable states (e.g., glassy, high-entropy) instead of more thermodynamically stable conditions. As a result, these methods provide new degrees of freedom.

4) **For the same reasons as in 2) and 3), as-synthesized nanoparticles are ligand-free, isolated, and with narrow size distribution,** as these reactions are typically quick and in solid-state, in contrast to the chemically synthesized materials in solutions.

Below we summarize emerging ultrafast synthesis methods, introduce their basic operating mechanisms, and review their application in sustainable energy and environmental technologies. These methods will play an increasingly important role in new materials R&D for emerging energy and environmental technologies.
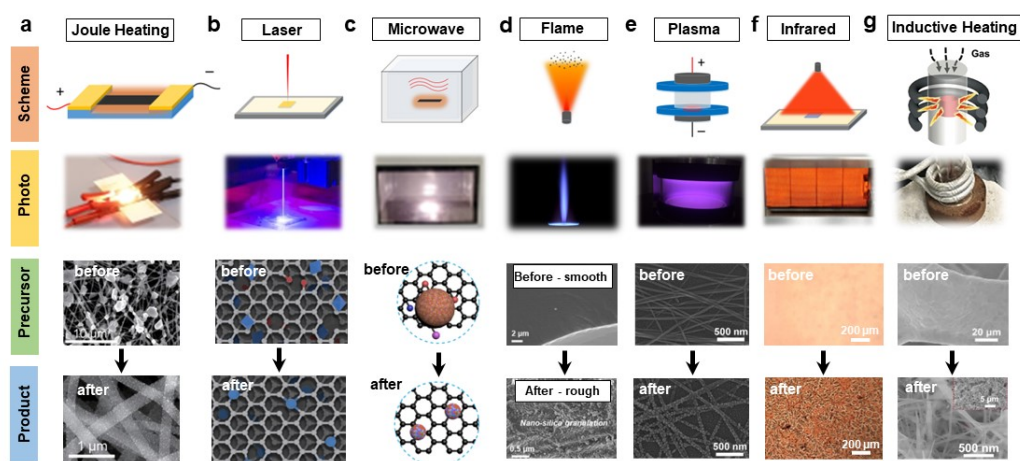

Fig. 2 Introduction of typical ultrafast manufacturing methods. Each row represents one ultrafast manufacturing method. **a.** ultrafast joule heating synthesis of nanoparticles. Reproduced with permission.[25] Copyright 2021, John Wiley & Sons, Inc. Reproduced with permission.[43] Copyright 2018, The American Association for the Advancement of Science. **b.** ultrafast laser synthesis of single atoms on graphene. Reproduced with permission.[44] Copyright 2019, American Chemical Society. Reproduced with permission.[45] Copyright 2021, Springer Nature. **c.** ultrafast microwave synthesis of nanoparticles. Reproduced with permission.[27] Copyright 2019, John Wiley & Sons, Inc. Reproduced with permission.[46] Copyright 2021, American Chemical Society. **d.** Flame treatment for poly(dimethylsiloxane) (PDMS) surface modification. Reproduced with permission.[28] Copyright 2019, AIP Publishing Inc. Reproduced with permission.[47] Copyright 2021, American Chemical Society. **e.** oxygen plasma treatment for Ag nanowire oxidation. Reproduced with permission.[29] Copyright 2017, Elsevier Ltd. Reproduced with permission.[48] Copyright 2021, Royal Society of Chemistry. **f.** flash infrared assisted perovskite thin films fabrication. Reproduced with permission.[49] Copyright 2021, American Chemical Society. Reproduced with permission. [50] Copyright 2019, Elsevier Ltd. **g**. rapid inductive heating synthesis of electrocatalysts on Ni foam. Reproduced with permission.[40] Copyright 2021, John Wiley & Sons, Inc.

To understand the recent development of ultrafast synthesis technologies in energy and environmental applications, we briefly introduce their basic principles. Representative ultrafast synthesis methods include Joule heating, laser-assisted synthesis, microwave-assisted synthesis, flame synthesis, plasma-assisted synthesis, infrared radiation-assisted synthesis, and inductive heating induced synthesis. These techniques are illustrated in **Fig. 2a-g**, respectively. Below we introduce the operational mechanisms and unique characteristics of these methods.

1) **Joule heating:** Joule heating methods use a pulsed current to heat target materials (**Fig. 2a**). In this process, a conductive substrate with appropriate resistance (e.g.,

carbon substrate) is rapidly heated up through flowing current and electronic scattering. Ideally, this process should be carried out in an inert atmosphere to minimize possible damage to the heater. The heat treatment is highly controllable and can be as fast as 10^5 K/s, rapidly heating the precursors to a few thousand Kelvin within milliseconds and producing target materials.[43] Moreover, this technique is programmable, effectively tuning the heating and cooling rate in the material synthesis process.[52] Joule heating involves three typical forms of reaction: *in-situ* synthesis,[43] contact synthesis,[31] and non-contact (radiative) synthesis.[53] Using these methods, researchers can create structures such as nanoparticles,[54] nanowires,[25,55] single atoms,[56,57] high-entropy alloys,[41,58] thin films,[59] and bulk ceramics[31]. The synthesis of bulk materials using ultrafast joule heating is usually pressure-free, unlike conventional sintering methods such as hot-pressed sintering.

2) **Laser:** Laser-assisted synthesis technologies involve a crucial step of the photothermal process where laser energy is transferred to lattice vibration through light-matter interactions (**Fig. 2b**). Conventionally, laser-assisted manufacturing technologies have been widely adopted in applications such as welding,[60] scribbling,[61] cutting,[62] drilling,[63] additive manufacturing, etc.[64,65] The high-speed, high-energy nature of lasers allows melting and even ablation of metals, ceramics, polymers, and composite materials. When the incident laser beam heats the target material, it may induce the generation of droplets (at micro- and nano-scales), vapor (at atomic scales), and plasma.[66] The above intermediates then mix, react, cool down, and condense into desired products (e.g. nanoparticles). A particular advantage of laser-assisted techniques is their high spatial and temporal resolution, allowing precise and controllable fabrication of nanomaterials and nanostructures in desired applications.[67-72]

3) **Microwave:** Microwave-assisted methods (**Fig. 2c**) utilize high-frequency electromagnetic radiation (e.g., microwave) as an energy source and convert it into heat rapidly, which turns precursors into desired products. The principle of energy conversion is the excitation of electron oscillation (of target materials) at the microwave source frequency. Microwave-absorbing materials, such as oxides and carbon materials, can rapidly heat up (~a few seconds) under microwave irradiation, which serves as either target materials or mediative heaters to synthesize precursors around them. The advantages of microwave-assisted methods include quick start-up and stopping, rapid heating, non-contact heating, etc. Unlike conventional furnace heating via radiant or convective heat flows, microwave heating does not entirely rely on heat convection but intrinsic heat conversion/generation. Thus, the heating efficiency and response are much higher than conventional methods, where massive furnace elements must be heated. Researchers can use this method to create nanoparticles,[73] core-shell structures,[74] 1D structures,[75] etc.[76-78] However, the reproducibility of microwave-assisted methods remains controversial, limiting their broad application for scalable synthesis and manufacturing.

4) **Flame:** Flame synthesis utilizes a flame to convert precursors to products via combustion reactions.[79] During the synthesis, the precursors can be fed into the reactor through gas or liquid. Accordingly, it can be divided into two categories,

namely vapor-fed aerosol flame synthesis (VAFS) and liquid-fed aerosol flame synthesis (LAFS) (**Fig. 2d**). For VAFS, low boiling point precursors enter the flame with a carrying gas, while for LAFS, solid precursors are carried through a suitable solvent and sprayed into the flame. In a typical LAFS process, aerosol droplets undergo evaporation, solution concentration, drying, thermolysis of precursor, microporous particle formation, and densification to the final particle (product). In the pyrolysis process, particles can rise to a high temperature (800 - 1600 K) within milliseconds to seconds and then quickly cool down. The high-temperature flame provides a heat source, chemical environment, and controlled residence time (in seconds) for the formation and evolution of the solid particle product. Flame synthesis methods are mainly used for (oxide) particle synthesis (primary and secondary particles such as aggregated or agglomerated particles); they can also be applied for thin-film synthesis and surface modifications.[28,80,81]

5) **Plasma:** A plasma is a partially ionized gas with charged and energetic species such as ions, electrons, photons, radicals, neutral species, etc. The synthesis process benefits the synergistic contribution of highly reactive energetic species and convective thermal energy (background gas temperature), dissociating the precursor for subsequent reactions. When plasma flux passes over the sample, the synthesis process starts rapidly; after the flux moves away, the reactive species and thermal energy dropped abruptly, leading to prompt cooling.[82,83] Due to its unique features, plasma-assisted techniques are extensively used for materials modifications such as reduction, oxidation, etching, coating, etc (**Fig. 2e**). For nanoparticle synthesis, the rapid and extensive energy release nature of plasma-assistance techniques are beneficial for small nanoparticle formation, avoiding Oswald ripening from conventional thermal synthesis. Plasmas can also directly react with surfaces of materials/particles, forming a wide range of materials, including metals, oxides, carbides, nitrides, and sulfides. Plasma-assisted techniques can synthesize nanoparticles,[84] thin films,[85] and even functionalize porous materials with pores larger than 10 μm.[36]

6) **Infrared:** Infrared-assisted synthesis uses infrared (IR) radiation to rapidly heat the precursors or other desired samples (**Fig. 2f**).[50] The heating process occurs through convective and radiative thermal energy, where the incident IR emission induces interband electronic transition in semiconductors and intraband transitions in metals. IR techniques are widely used in applications such as IR drying, atomic-layer deposition, and 3D printing techniques. The samples and IR sources are usually placed between two reflecting layers for high heating rate and energy efficiency. This method is non-contact, radiative, easily accessible, and subject to a scalable roll-to-roll process.[86] However, since the energy input of IR-assisted methods can be non-uniform and directional, these methods are most suitable for thin films,[87,88] surfaces,[89,90] layer-by-layer fabrication,[91] and nanomaterials preparations.[92-96]

7) **Inductive heating**: inductive heating is a process that utilizes eddy currents generated in conductive metal substrates through electromagnetic induction (**Fig. 2g**). When a closed conductor is placed in an alternating magnetic field, an induced current (eddy current) is generated preferably on the surface of the conductor, heat

the sample via electronic scattering (analogous to joule heating). This technique has been widely used in materials processing, such as hardening, annealing, and welding. The inductive heating process is non-contact, fast, scalable, clean, efficient, and controllable, and it can be utilized to make a wide range of materials.[97-103] This method is effective when the synthesis substrates are metals, particularly if in 3D, such as nanoparticles loaded on nickel foam for energy applications. However, it may not be as useful as other previously mentioned ultrafast synthesis methods, when non-metal substrates or no even substrates are needed in target applications.

From the descriptions, we note there are inherent correlations between the working mechanisms of the above ultrafast synthesis techniques. All the techniques allow rapid energy conversion from one form to heat. For example, the essence of joule heating, microwave heating, and inductive heating is the electronic scattering-induced joule heating within the target materials. The laser and Infrared method utilizes the photothermal effect, which converts photo energy into heat. Plasma and flame synthesis involves reactive species, radicals, and convective thermal energy. Besides the abovementioned methods, other field-assisted synthesis/sintering techniques include spark plasma sintering,[104-107] flash sintering,[108-110] electron beam assisted methods,[111] UV-assisted sintering.[112-114] These techniques share the same general ultrafast synthesis principle that uses one or multiple fields as an energy source to drive desired chemical reactions. Together, these methods provide a powerful toolbox for a sustainable future.

The choice of precursors is vital to the successful synthesis via ultrafast techniques. Due to the instantaneous energy release and fast reaction nature of the ultrafast synthesis methods, two general principles in selecting precursors should be noted. First, the precursors should obtain relatively high reactivity; this means they are either easily decomposable or reactive with other reactants. For example, metal nitrides and metal acetates are usually chosen as precursors for nanoparticle synthesis, as they decompose at a few hundred Celsius. Second, the precursors are ideally responsive to external thermal/optical/electric/magnetic fields. For instance, microwave absorbents are preferred precursors in microwave-assisted techniques, and conductors are selected for inductive heating-assisted approaches. Note that ultrafast synthesis techniques provide energy to precursors either directly or indirectly. Depending on the requirement for the final product, the precursors should fulfill the first rule but not necessarily the second.
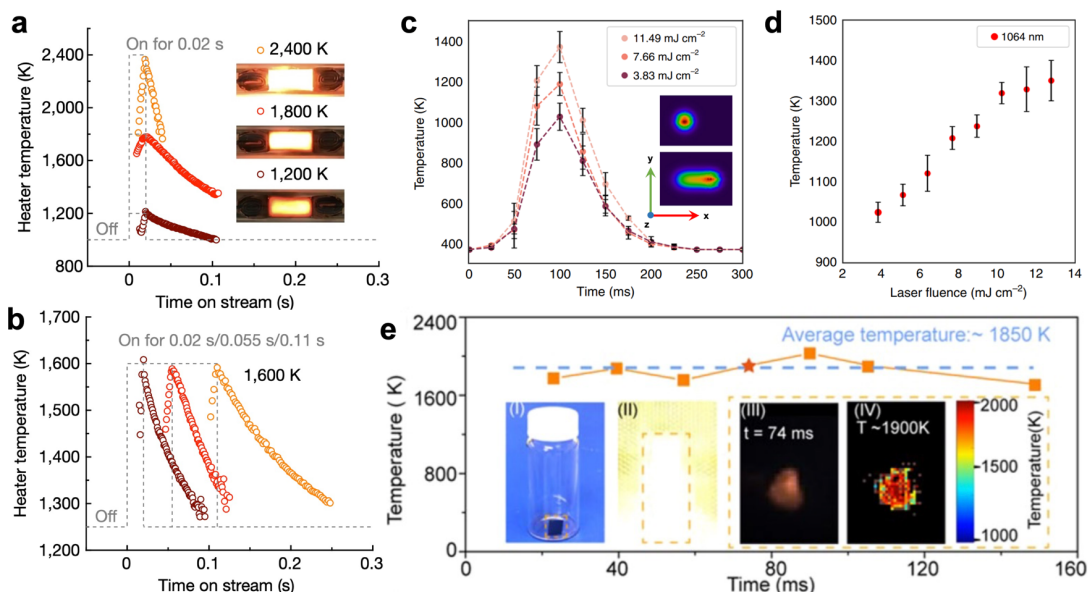
Fig. 3 Temperature control for ultrafast technologies. The temperature profile of joule heating adjusted by **a** electrical input power and **b** pulse duration; Temperature profile of laser-assisted technique. Reproduced with permission.[52] Copyright 2022, Springer Nature. **c** typical temporal thermal profiles and **d** peak temperature at different incident laser power. Reproduced with permission.[45] Copyright 2021, Springer Nature. **e** The temperature profile of precursor/substrate during microwave heating and inset are photo images and IR images of the samples. Reproduced with permission.[46] Copyright 2021, American Chemical Society.

The precise control of temperature (temporally and spatially) is crucial for ultrafast synthesis methods, as the synthesis of most materials (if not all) is sensitive to temperature (heat treatment). In general, all the ultrafast synthesis techniques discussed in this article have comparably fast temperature response to conventional methods. However, the degree of heating/cooling response and spatial resolution can be quite different in each technique. To illustrate the temperature control ability of ultrafast synthesis methods, we choose three typical techniques as examples for discussion. Joule heating utilizes a resistor as a heater and electricity as an energy input for temperature control. As a result, the temperature response of the heater is mainly determined by the duration (program) of electricity and the resistor's heat capacity/thermal conductivity. Representative temperature profiles via joule heating are illustrated in Fig. 3a and b. The two figures demonstrate that by varying the input power (Fig. 3a) and pulse duration (Fig. 3b), both maximum temperature and heating/cooling profile can be precisely controlled and significantly altered.[52] However, unless microfabrication techniques are utilized to obtain joule heaters, the heating resolution of joule heating-based techniques may be limited as most reported literature uses heaters at least at millimeter scales.

In contrast, laser-assisted techniques obtain a highly controllable spatial and temporal resolution, as a highly focused laser beam provides the heating. As shown in Fig. 3c and d, both the temperature profile (Fig. 3c) and peak temperature achieved (Fig. 3d)

are determined by the laser power of a single emission. The temperature and spatial resolution of the laser can also be tuned in a certain range by the focus of the laser. In addition, even with the same laser power, the authors demonstrated that the maximized temperature was tunable with multiple laser emissions.[45] Microwave-assisted techniques are less controllable than the above two techniques but still obtain instant high temperatures and maintain a relatively stable temperature profile. Fig. 3e shows the temperature profile of a microwave-heated reduced graphene thin film, which kept an average temperature at about 1850K for 160 ms.[46] However, as the microwave field may not be even in the reaction chamber, the reproducibility of microwave-assisted methods may be a concern. In summary, the synthesis temperature via ultrafast-assisted techniques can be finely adjusted, facilitating precise materials synthesis and discovery. Furthermore, we discussed the pros and cons of typical ultrafast methods, indicating the choice of ultrafast synthesis techniques can play an essential role in as-synthesized materials.
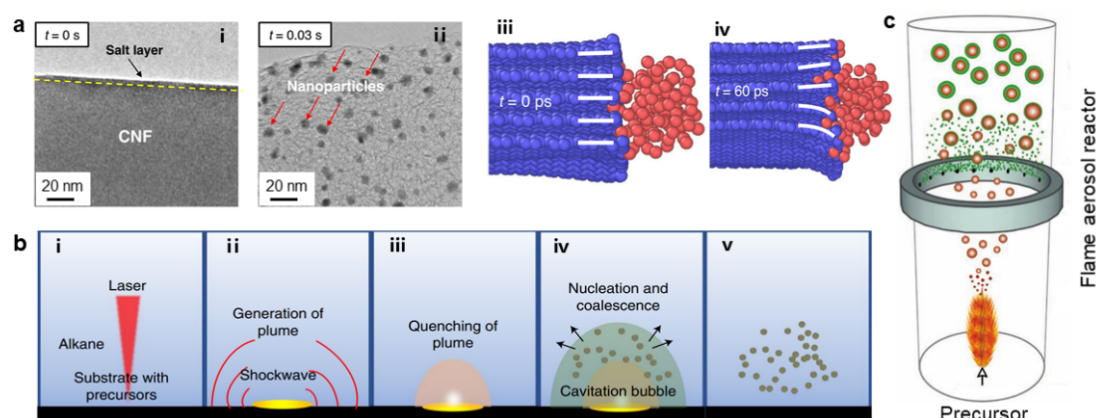

Fig. 4 Process and synthesis mechanism of typical ultrafast synthesis techniques. a *In situ* TEM images of Joule heating nanoparticle synthesis process (i, ii) Molecular dynamic modeling of Pt cluster residing in edge planes at 1800 K, before and after 60 ps time relaxation. Reproduced with permission [115] Copyright 2020, Springer Nature. **b** A schematic depicting the formation mechanism of nanoparticles by the laser scanning ablation method: laser generation (i), light-matter interaction (ii), plume expansion (iii), bubble generation (iv) and bubble collapse (v). Reproduced with permission.[116] Copyright 2022, Springer Nature. **c** Schematic illustrating the synthesis of core-shell nanoparticles by flame synthesis. Reproduced with permission.[117] Copyright 2010, John Wiley & Sons, Inc.

We now introduce materials synthesis mechanisms for a few typical ultrafast methods. In order to create materials with unusual structures or exceptional properties, these techniques feature both rapid heating and rapid cooling rates. **Fig. 4a** illustrates ultrafast synthesis of nanoparticle before and after joule heating through in situ TEM study and MD simulation.[115] As shown in **Fig. 4a-i**, a layer of precursor salt (H_2PtCl_6) can be uniformly loaded on the amorphous carbon fiber (smooth surface). After joule heating for 30 ms, the surface roughness of carbon fiber increased drastically, and it was loaded with large amount of as-synthesized, monodispersed Pt nanoparticles **(Fig. 4a-ii)**. Because the heating process was rapid, the amorphous carbon could not be

fully graphitized, and it turned into highly defective turbostratic graphite instead. The large number of defect sites offer ideal nucleation centers for nanoparticles, and they anchor them firmly. More intriguingly, from the MD simulations, as the Pt particles are loaded on defect edge sites of graphite, their Pt atoms can slightly intercalate into the graphene planes. This phenomenon results from the large charge transfer and the high binding energy between Pt and defect sites on graphite, where the binding energy of Pt/Carbon (-8.51 eV/atom) is even greater than that of Pt-Pt (-5.37 eV/atom). This comparison explains the excellent thermal stability of joule heating synthesized carbon loaded nanoparticles, where agglomeration of nanoparticles can barely occur, even at relatively high temperatures, demonstrated both in experiments (~1200 K) and MD simulations (1800 K, **Fig. 4a**-iii, iv)). Joule heating is also well-known for multi-elemental and high entropy materials synthesis.

A common feature of ultrafast synthesis is that the precursors are exposed to instantaneous high power, when a large amount of heat is generated and released, decomposing the precursors and forming desired products. Similarly, **Fig. 4b** illustrates the ultrafast synthesis process of the laser scanning ablation method in alkane solution for (high-entropy) nanoparticle preparation in times as short as nanoseconds.[116] This process can be understood as a photothermal evaporation process. When the laser interacts with precursor salts **(Fig. 4b-i, ii)**, they quickly decompose into a mixed vapor of ions, atoms, and gases **(Fig. 4b-iii)**, which is rapidly cooled down by the surrounding alkane solution, and finally solidifies to nanoparticles **(Fig. 4b-iv,v)**. The size of the nanoparticles can be tuned with the light-matter interaction time. In other cases, by sophisticated design of ultrafast synthesis reactors and the relevant chemical reactions, complex structured functional nanoparticles can be synthesized. **Fig. 4c** shows the scheme of a scalable, one-step ultrafast synthesis setup of Ag/SiO$_2$ core-shell nanoparticles.[117] In addition to a regular burner for Ag nanoparticles flame synthesis, a ring to inject SiO$_2$ precursor vapor can be added, leading to an in-flight SiO$_2$ coating on fresh flame-synthesized Ag nanoparticles. By tuning the distance between the metal ring and the flame and/or the concentration/flow rate of the SiO$_2$ precursor, the size and coating thickness of the core-shell nanoparticles can be further adjusted. The above examples reveal unique characteristics of ultrafast synthesis techniques, and they inspire materials design and discovery in desired applications in the future.
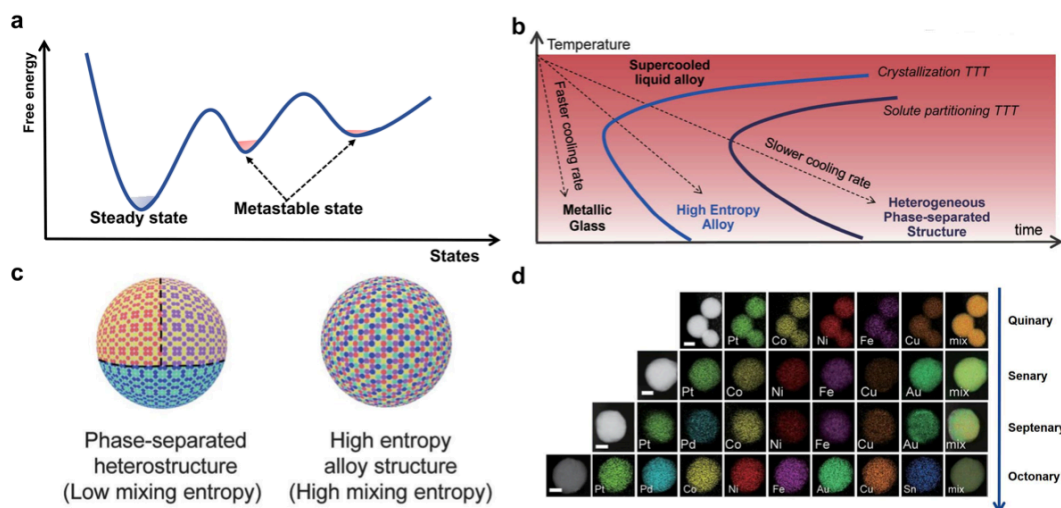
Fig. 5 Characteristics of ultrafast synthesized metastable materials. a. Free energy vs. states of a certain material. **b.** Time-temperature-transformation (TTT) diagram showing the kinetic process in forming metastable and steady-state phases. **c.** Comparison of multielemental particles: phase-separated heterostructure vs. high entropy alloy structure. **d.** HAADF TEM images and STEM elemental mapping of HEA-NPs: quinary (PtFeCoNiCu), senary (PtCoNiFeCuAu), septenary (PtPdCoNiFeCuAu), octonary (PtPdCoNiFeCuAuSn). Reproduced with permission.[43] Copyright 2018, The American Association for the Advancement of Science.

Another unique feature of ultrafast synthesis techniques is that they can create metastable states of materials in a facile manner (**Fig. 5a**). Compared with their thermodynamically stable counterparts, metastable materials, such as high entropy materials for structural alloys,[118-120] electrocatalysis,[55,121] and energy storage,[122,123] may exhibit outstanding properties. Preparing such metastable materials can be a daunting task for conventional materials synthesis, where there is often enough time for elemental diffusion, leading to more thermodynamically stable materials. Ultrafast synthesis methods provide a unique solution to this problem, where the samples can be cooled sufficiently quickly. To illustrate this phenomenon, the classic time-temperature-transformation (TTT) diagram for metallurgy is shown in **Fig. 5b**. In conventional thermal approaches with a slow cooling rate and long elemental diffusion time, phase-separated materials are usually formed (**Fig. 5c**). In contrast, ultrafast synthesis with high cooling rate can generate supercooled liquid alloys to form metastable multimetallic alloys or even metallic glass at rapid solidification. As a result, high entropy alloy nanoparticles (HEA-NPs), including quinary (PtFeCoNiCu), senary (PtCoNiFeCuAu), septenary (PtPdCoNiFeCuAu), and octonary (PtPdCoNiFeCuAuSn), can be readily prepared as shown in **Fig. 5d**.
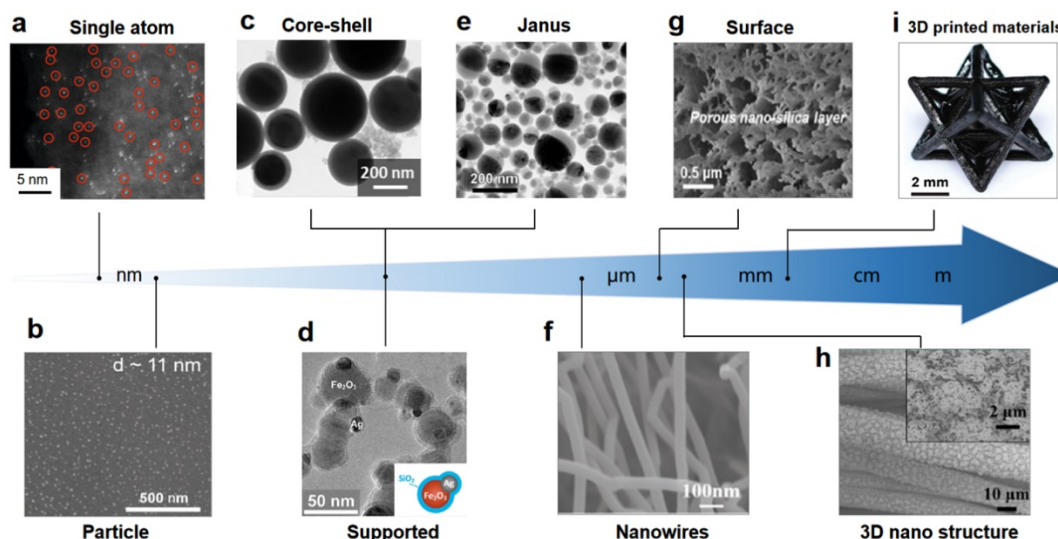
Fig. 6 Ultrafast materials synthesized materials across length scales. a. HAADF-STEM image of isolated Pt atoms deposited on a laser-reduced graphene oxide support. Red circles indicate atomic locations. Reproduced with permission.[45] Copyright 2021, Springer Nature. **b**. SEM image of particles on carbonized wood channels via microwave treatment. Reproduced with permission.[27] Copyright 2019, John Wiley & Sons, Inc. **c**. TEM image showing FeNi@SiO$_2$ core-shell particles by flame synthesis. Reproduced with permission.[124] Copyright 2022, American Chemical Society. **d.** TEM image of Fe$_2$O$_3$ supported Ag particles with SiO$_2$ coating via flame synthesis. Reproduced with permission.[125] Copyright 2011, American Chemical Society. **e.** TEM image of the Fe$_2$O$_3$‖SiO$_2$ Janus particles by flame synthesis. Reproduced with permission.[126] Copyright 2009, John Wiley & Sons, Inc. **f**. SEM image of Si nanowires turned from wasted Si microparticles after joule heating. Reproduced with permission.[25] Copyright 2021, John Wiley & Sons, Inc. **g.** SEM image showing microstructure and surface morphology of flame treated PDMS foam. Reproduced with permission.[47] Copyright 2021, American Chemical Society. **h.** SEM image of NiMo alloy film deposited on carbon paper after N$_2$ plasma treatment. Reproduced with permission.[127] Copyright 2016, John Wiley & Sons, Inc. **i.** photo images of 3D printed SiOC after ultrafast high-temperature sintering. Reproduced with permission.[31] Copyright 2020, The American Association for the Advancement of Science.

Ultrafast synthesis methods can prepare materials across multiple length scales from (sub)nanometer to millimeter, as illustrated in **Fig. 6** and with tunable structures from 0D to 3D, such as single atoms, (core-shell) nanoparticles, nanowires, porous materials, thin films, surfaces, and even 3D printed bulk samples. **Fig. 6a** is a high-angle, annular, dark-field scanning transmission electron microscopy (HAADF-STEM) image of single-atom Pt on reduced graphene oxide support, synthesized with laser-assisted pyrolysis and reduction of freeze-dried graphene oxide film loaded with chloroplatinic acid (H$_2$PtCl$_6$) (up to 1692.2 K, ~1 ms).[45] **Fig. 6b** shows metal oxide (CoO$_x$) nanoparticles rapidly fabricated inside 3D carbonized wood channels after microwave-assisted methods. These nanoparticles are ultrasmall (~11 nm), uniform, and monodisperse (synthesized at ~2200 K, 4 s). Besides single component/phase nanoparticles, nanoparticles with complex structures can also be synthesized with ultrafast methods.[27] **Fig. 6c-e** shows three TEM images of structured nanoparticles

prepared by one-step flame synthesis: FeNi@SiO_2 core-shell structured nanoparticles (**Fig. 6c**),[124] Ag/Fe_2O_3 supported nanoparticles with SiO_2 coating (**Fig. 6d**, dark particles represent Ag),[125] and Fe_2O_3/SiO_2 Janus nanoparticles (**Fig. 6e**).[126] Ultrafast methods can synthesize more than (nano/microstructured) particles. **Fig. 6f** shows the synthesis of nanowires using the joule heating method. This technique transformed photovoltaic Si waste microparticles and reduced graphene oxide composite into silicon nanowire (SiNW) electrodes for lithium-ion batteries (LIBs) in a few milliseconds (~2100 K, 10 ms).[25] **Fig. 6g** shows a rapid flame surface treatment method that can treat and tune the surface properties of polymeric foams (sensitive substrate). This method successfully formed a superhydrophobic surface with nano-silica rough structures, while maintaining a soft/stretchable polydimethylsiloxane (PDMS) skeleton. The pyrolysis of PDMS molecules can be adjusted by changing the flame scanning speed, thus effectively customizing the surface roughness (1300 °C, 1~3 s).[47] In addition to flame treatment methods, where the treated surface areas are macroscopic, non-directional methods such as plasma treatments can fine-tune the surfaces of microstructures. Using a rapid N_2 plasma activation method, NiMo bimetallic nanoparticles can be tuned into NiMoN, even within a porous 3D nanostructured film (**Fig. 6h**) (450 °C, 15 min).[127] The as-synthesized materials demonstrate outstanding hydrogen evolution reaction (HER) performance of small overpotential and long duration. Moreover, ultrafast techniques can also generate complicated structures within bulk materials. Through Joule heating, 3D printed silicon oxycarbide (SiOC) precursor was rapidly sintered to polymer-derived ceramics with uniform shrinkage and well-maintained structures, as shown in **Fig. 6i** (1200 °C, 10 s).[31] Various materials and structures can be rapidly prototyped and synthesized with these methods, facilitating materials discoveries in many applications.

2. Ultrafast Synthesis for Energy and Environmental Applications

The unique benefits of ultrafast synthesis open up new possibilities for emerging renewable energy and environmental applications. Below we will introduce representative works in studying renewable energy (energy storage, energy conversion) and environmental applications (gas purification, water purification and solid waste recovery) using ultrafast materials synthesis techniques.
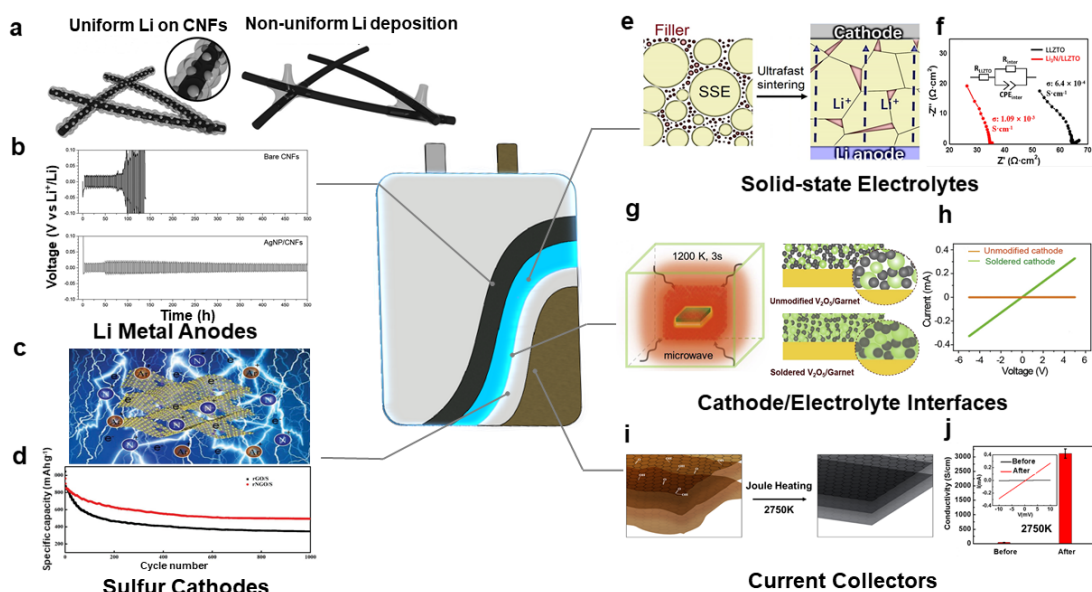
2.1 Energy Storage

Fig. 7 Ultrafast synthesis for batteries. a. Anode-Schematic of joule heating synthesized Ag nanoparticle seeds on carbon current collectors for high-performance Li batteries. **b.** Cycling performance of Li anode plating/stripping at 0.5 mA cm^{-2} for 1 mAh cm^{-2} on bare CNFs and AgNP/CNFs. Reproduced with permission.[128] Copyright 2017, John Wiley & Sons, Inc. **c.** Cathode-Schematic representing plasma-assisted reduced nitrogen-doped graphene (rNGO). **d.** Cycling performance of rGO/S and rNGO/S composite cathodes for 1000 cycles at a charging rate of 1.0 C. Reproduced with permission.[129] Copyright 2019, John Wiley & Sons, Inc. **e.** Electrolyte-schematic of the ultrafast sintering of LLZTO SSE and Li$_3$N filler. **f.** Electrochemical impedance spectroscopy (EIS) of LLZTO and Li$_3$N/LLZTO. Reproduced with permission.[130] Copyright 2021, American Chemical Society. **g.** Interfaces-Schematic illustration of the rapid microwave soldering process of the cathode/SSE interface. **h.** I-V curves of the cathode layers. Reproduced with permission.[131] Copyright 2020, Elsevier Inc. **i.** Current collector-Schematic illustrating the Joule heating process of reducing GO to the RGO. **j.** The conductivity of RGO film before and after the rapid 2750 K reduction. Inset shows the linear scan of the I-V curve. Reproduced with permission.[59] Copyright 2016, American Chemical Society.

This section introduces ultrafast synthesis techniques for two representative electrochemical energy storage technologies: Li-(ion) batteries and super/pseudocapacitors. Similar principles may be applied to other electrochemical systems such as Na-(ion) batteries or Zn-(ion) batteries. Li-(ion) batteries contain an anode, a cathode, a (solid) electrolyte, electrode/electrolyte interfaces, and current collectors. Ultrafast synthesis techniques can play vital roles in solving problems in each part, as shown in **Fig. 7**.

The quest for energy-dense batteries suggests the use of Li metal anodes, but Li dendrite penetration of the electrolyte (leading to short circuits) impedes their practical application.[132,133] A 3D lithium metal matrix anode in ultralight carbon seemed a promising solution. Still, the lithophobic carbon matrix leads to inhomogeneous nucleation and growth of Li metal dendrites, leaving the dendrite

problem unaddressed. The problem can be alleviated by synthesizing homogeneously dispersed ultrafine Ag nanoparticles (AgNPs) on carbon nanofibers (CNFs) via the Joule heating method, as depicted in **Fig. 7a**.[128] The high temperature promotes the formation of a strong bond between AgNPs and the carbon substrate, as we discussed earlier.[115] At the same time, the ultrafast process facilitates homogeneous particle dispersion, uniformly seeding and depositing Li on CNFs substrate, leading to a stable cycling performance (**Fig. 7b**). Silicon is another attractive anode material for next-generation LIBs due to its excellent specific capacity. Jae et al.[134] introduced a cost-effective IR-assisted ultrafast processing strategy that improves Si anode's cycle stability and rate capability. The sustained capacity of IR flash-treated sample at a high rate of 5 A g^{-1} was 70% higher than conventionally dried samples. The tunable flash processes lead to selective binder carbonization, Si surface modification, and porosity distribution design, which enhance the overall performance of the electrode. This IR-assisted ultrafast technique addresses the problem of Si anode without using costly synthetic functional binders or delicately designed nanomaterials showing great promise in the fabrication and manufacturing of battery electrodes.

Sulfur has attracted considerable attention as a cathode due to its high theoretical specific capacity (>1600 mAh g^{-1}). However, practical application of Li-S batteries faces significant challenges, such as poor electronic and ionic conductivity of active cathodes, the considerable volume change of sulfur, and polysulfide intermediates (Li_2S_n, $2 < n \leq 8$) shuttling. To overcome these problems, Lu et al.[129] prepared a 3D N-doped graphene porous framework (rNGO) by hollow cathode discharge (HCD) plasma technology under the flow of argon and nitrogen (**Fig. 7c**). N_2 and Ar were ionized to e$^-$, N$^+$, and Ar$^+$ in this process. N$^+$ was then reduced and doped into rGO within 15 min of the plasma discharge treatment. The plasma-assisted N-doped rNGO/S cathode cycled 1000 times at the rate of 1.0 C with 578 mAh g^{-1} remaining capacity, showing much better cycling stability than the undoped rGO/S (**Fig. 7d**). The outstanding performance is attributed to 3D rNGO's ability to anchor soluble Li polysulfide at sufficiently high binding energy to inhibit the shuttle effect, provide a pathway for ion migration, improve electrical conductivity, and adapt to volume expansion during charge and discharge.

Solid-state batteries (SSBs) using solid-state electrolytes (SSEs) are considered next-generation energy storage technology, potentially bringing better safety and higher energy density than LIBs with liquid electrolytes. In particular, oxide ceramic SSEs have attracted significant attention as they may have high ionic conductivity (~1 mS/cm) and a wide electrochemical stability window.[135] However, the solid-solid contact between SSE particles and cathode particles is poor, limiting ion transport and, therefore, the performance of SSBs. To address the unavoidable gap between these solid particles, the addition of appropriate fillers has been tried. Li_3N is a good sintering agent and would be an ideal filler for composite materials because of its suitable ionic conductivity (10^{-4} S cm^{-1}) and low electrical conductivity (10^{-12} S cm^{-1}). Unfortunately, its use has been hindered by its high volatility.[136,137] Hu et al.[130]

solved this problem using the Joule heating method in adding Li_3N as a sintering agent to Ta doped $Li_7La_3Zr_2O_{12}$ (LLZTO) SSE (**Fig. 7e**). Although the process occurred at 1600 K, only 20 seconds was required for rapid heating and cooling (~10^2 K/s), minimizing material volatilization. As shown in **Fig. 7f**, electrochemical impedance spectroscopy (EIS) measurements show that the ionic conductivity increased from 6.4×10^{-4} S cm^{-1} to 1.09×10^{-3} S cm^{-1} after Li_3N was added to the LLZTO. For SSE-cathode interfaces, Hu et al.[131] demonstrated a rapid high-temperature microwave heating method that reduced the interfacial resistance between V_2O_5 cathode and Garnet $Li_7La_3Zr_2O_{12}$ (LLZO) SSE (**Fig. 7g**). The microwave-assisted welding method can selectively melt granular V_2O_5 and re-solidify it in seconds, quickly forming a complete and continuous cathode layer with the SSE and carbon black (CB), improving electronic and ionic conductivity of the cathode. Compared to the unmodified cathode, the modified sample shows a remarkable 690-fold increase of electronic conductivity (**Fig. 7h**) and a 28-fold decrease of cathode/SSE interface resistance, which is highly desired for all-solid-state batteries.

Current collectors (CC) play a crucial role in batteries, yet might be the least studied part. CC are made of copper (Cu) and aluminum (Al) foils for anodes and cathodes, respectively, accounting for 15-50% of the total weight of batteries. As a result, mechanically robust, lightweight, highly electronically conductive, inexpensive, and electrochemically inert films are highly desired.[138] Conductive carbon films composed of graphene or reduced graphene oxide (RGO) nanosheets hold promise because of their relatively high conductivity, low density, and abundant sources. However, their electrical conductivity is usually less than 1,000 S/cm, much lower than that of metals, due to the incomplete reduction of functional groups and defects on graphene films. To overcome this problem, Hu et al. utilized Joule heating at ultra-high temperature (~ 2750 K) for a short time (1 min) (**Fig. 7i**), significantly enhancing the conductivity of a RGO film to 3112 S/cm RGO (**Fig. 7j**).[59] The high temperature thoroughly reduced the RGO but also assisted in healing the RGO defects.
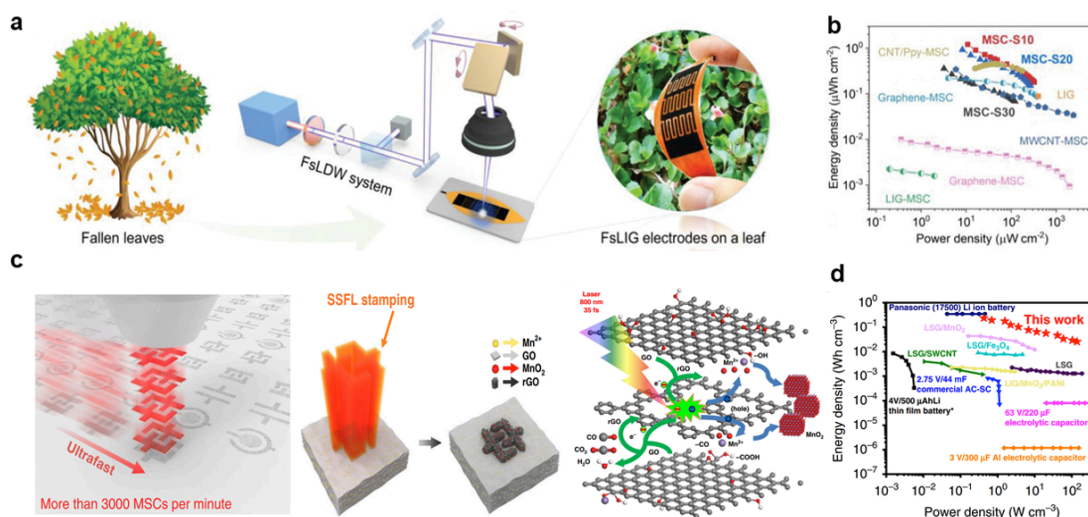
Fig. 8 Ultrafast manufacturing for super/pseudocapacitors. a. Schematic exhibiting the fabrication process of femtosecond laser-induced graphene (FsLIG) on fallen leaves at ambient condition. **b.** Comparison of the energy-storage performance of the FsLIG-MSCs on leaf with the recently reported MSCs (Ragone plots). CNT: carbon nanotube; MWCNT: multiwall CNT. Reproduced with permission.[139] Copyright 2021, John Wiley & Sons, Inc. **c.** The ultrafast processing via spatially shaped femtosecond laser on hybrid GO films. **d.** Energy and power densities of the LIG/MnO$_2$ MSCs compared with other capacitors and batteries. Reproduced with permission. [140] Copyright 2020, Springer Nature.

High-performance super/pseudocapacitors have high power, simple structures, and are easily made flexible/wearable, potentially benefiting augmented reality and the metaverse.[141-144] For example, flexible graphene supercapacitors may provide high power density, long cycle life, excellent mechanical/electrochemical performance, and safe operating conditions as promising flexible/wearable power devices. Le et al. demonstrated a facile femtosecond laser-assisted method to make micro-supercapacitors (MCSs) on natural fallen leaves at a fast writing speed of 50 mm/s (**Fig. 8a**).[139] The lasers provide high temperature and induced mesoporous few-layered graphene as active materials, leading to a high areal capacitance of 34.68 mFcm^{-2} and 99% capacitance retention even after 50,000 charge/discharge cycles (**Fig. 8b**). More intriguingly, Jiang et al. utilized a spatially shaped femtosecond laser (SSFL) for high-throughput stamp fabrication of graphene/MnO$_2$ based MSCs on flexible substrates with single pulses (**Figs. 8c**).[140] Since 1,000 space-shaped laser pulses can be generated per second, more than 30,000 MSCs can be fabricated in merely 10 minutes. The energy and power densities of the MSCs exhibited excellent energy density of 0.23 Wh cm^{-3} and power density of 136 W cm^{-3} with stable cycling performance compared with other capacitors and batteries (**Fig. 8d**).
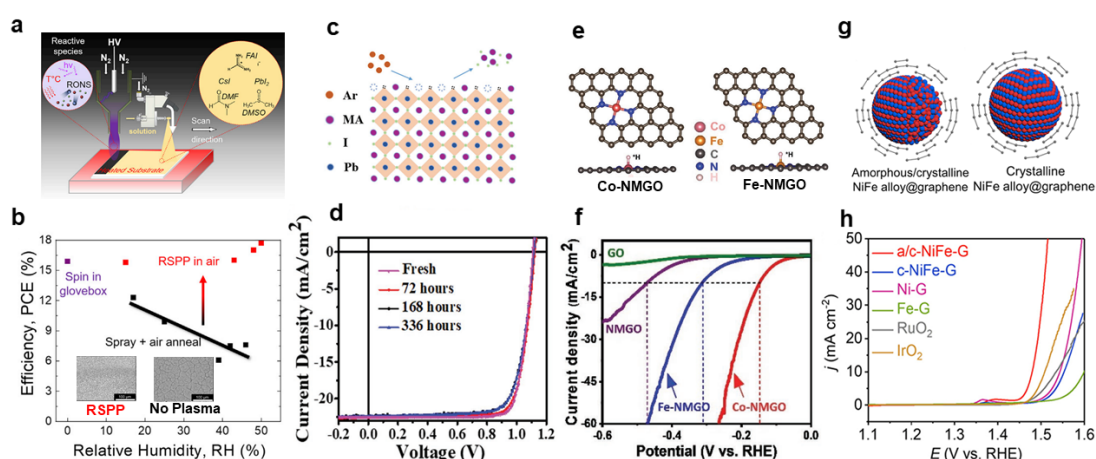
2.2 Energy Conversion

Fig. 9 Ultrafast synthesis of solar cells and water splitting. a. Plasma-assisted, open-air, and scalable fabrication of perovskite solar cells. **b.** Plot of power conversion efficiency (PCE) values vs. relative humidity (RH), where plasma-assisted synthesis shows higher PCE than conventionally synthesized samples. Reproduced with permission.[145] Copyright 2020, Elsevier Inc. **c.** Argon plasma treatment

(APT) for MAPbI₃ surfaces to remove methylammonium iodide (MAI) and expose the lead-rich underlayer. **d.** Stability test device exposed to air without encapsulation. Reproduced with permission.[146] Copyright 2018, John Wiley & Sons, Inc. **e.** Co-NMGO and Fe-NMGO SAC catalysts. **f.** Catalytic performance for HER LSV plots. Reproduced with permission.[147] Copyright 2021, John Wiley & Sons, Inc. **g.** Schematic shows structural models of a/c-NiFe-G and c-NiFe-G. **h.** LSV curves with 80% iR-correction of a/c-NiFe-G, c-NiFe-G, Ni−G, Fe−G, RuO₂, and IrO₂ were tested on a glassy carbon electrode. Reproduced with permission.[148] American Chemical Society.

Sustainable energy generation and conversion from solar cells and fuel cells are critical for clean energy utilization. Solar cells using metal halide perovskites have shown 25% Power conversion efficiency (PCE), outperforming amorphous silicon and organic photovoltaics. The lack of rapid, facile, and scalable fabrication processes for perovskite solar cells can hinder its broad application. Dauskardt et al. reported an atmospheric plasma route, combined with spray deposition, achieving an outstanding deposition rate of 12 m/min (**Fig. 9a**).[145,149] This scalable fabrication technique also gave a low defect density in the perovskite material, allowing it to achieve a high PCE (**Fig. 9b**) of 18.0% at $V_{OC} > 1.06V$. Huang et al. utilized the argon plasma technique (**Fig. 9c**), with treatment time as short as 2s, yielding an outstanding PCE of 20.4% with more than 300 hours stable (**Fig. 9d**) at ~50% humidity.[146] This remarkable result is due to the argon plasma's ability to rapidly remove undesired organic components on the perovskite surface without damaging the subsurface, facilitating enhanced charge collection.

In addition, the IR-assisted method is also widely used in the synthesis of perovskite films.[49,150-153] Graetzel et al. used infrared synthesis to study the phase transition of formamide lead triiodide (FAPbI₃) in solar cell applications.[154] By exploring different heating times to trigger the phase transition, the optimal film crystallization annealing time was only 640 ms. Under this condition, black FAPbI₃-based perovskite (additive-free) solar cells are highly stable with a power conversion efficiency (PCE) of 18.5% and 90% PCE retention after 1500h. More intriguingly, Huang et al. reported that the ultrafast annealing process can benefit from controlling the vacancy in semiconductor light absorbers, reducing charge recombination, and improving solar cell power output. A high-throughput fabrication of infrared annealed perovskite solar cell modules within 3 minutes is demonstrated.[26] In the CH₃NH₃PbI₃ module with an area of >20 cm², the average stable open-circuit voltage reaches to 1.19 V. The aperture efficiency reaches 17.8% in one sun and 18.7% in one-quarter of the sun illumination, respectively.

The hydrogen evolution reaction (HER) plays a vital role in producing hydrogen from electrochemical water splitting.[155,156] Nanosized catalysts are critical because they provide a high surface area. One key thrust substitutes non-noble metal catalysts for noble metal-based nanocatalysts. Notably, single-atom catalysts (SACs) provide an emerging solution for nanocatalysts since their surface-to-volume ratios are unparalleled.[45] Yang et al.[147] synthesized a SAC catalyst loaded on porous graphene

oxide (GO) using low-intensity pulsed laser irradiation (LI). As shown in **Fig. 9e**, after laser irradiation at ambient conditions, Co or Fe single atoms were loaded on mesoporous GO (NMGO) support, assisted by the support's dangling bonds. Linear sweep voltammetry (LSV) tested for different SAC catalysts in acidic medium of 0.5 M H_2SO_4 is shown in **Fig. 9f,** where SAC Co-NMGO exhibited an outstanding overpotential of 146 mV at a current density of 10 mA cm^{-2}, much better than that of commercial RuO_2 and IrO_2 at same testing conditions. Utilizing the same method, an excellent oxygen reduction reaction performance was also achieved with SAC Fe-NMGO, potentially benefiting the development of fuel cells and metal-air batteries.

The oxygen evolution reaction (OER) is another half-reaction that plays a critical role in energy and the environment (such as electrochemical water splitting,[157-160] metal-air batteries,[161-163] CO_2 reduction,[164-166] etc.). However, OER is a complex four-electron reaction with a large kinetic barrier and limited overall energy efficiency. Ultrafast synthesis can make R&D of the catalysts more practical. As shown in **Fig. 9g**, Graphene-coated NiFe alloy nanocomposites with unique amorphous/crystalline heterogeneous structures (a/c-NiFe-G) were synthesized by microwave thermal shock strategy.[148] **Fig. 9h** shows the linear sweep voltammetry (LSV) curves of a/c-NiFe-G, c-NiFe-G, Ni−G, and Fe−G prepared by a microwave-assisted process, where commercial RuO_2 and IrO_2 are used as references. The a/c-NiFe-G exhibits the lowest onset overpotential, 250 mV at 10 mA/cm^2. Compared to crystalline NiFe alloy@graphene, the amorphous counterparts have an inherent disorder and unsaturated coordination structures, leading to more abundant active sites and higher electrocatalytic performance.
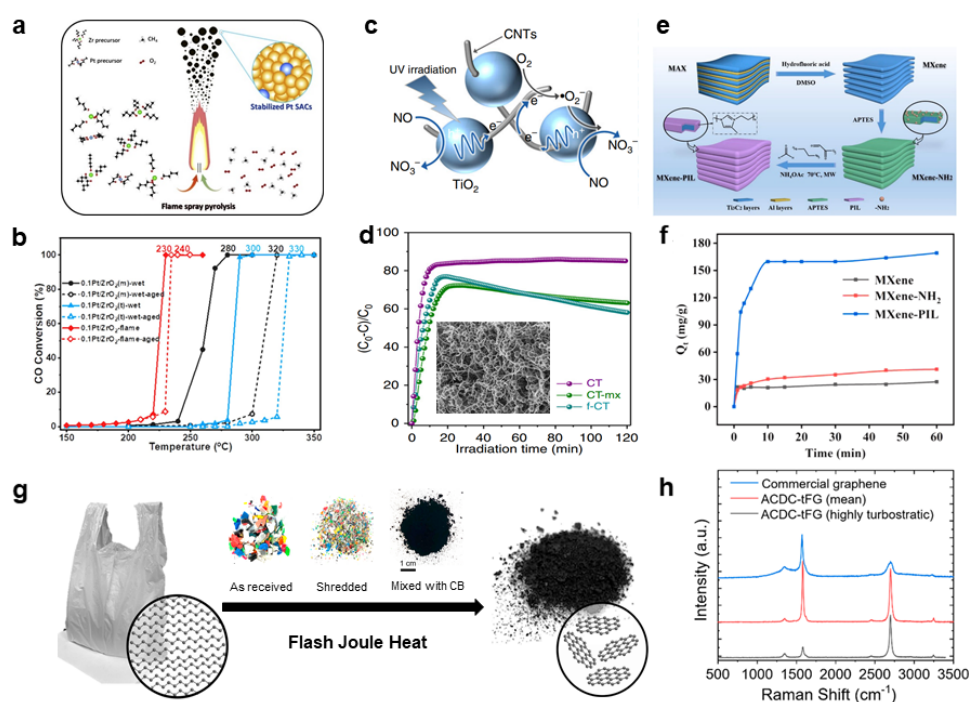
2.3 Environmental applications

Fig. 10 Ultrafast synthesis for the environment. a. The schematic of Pt single-atom catalysts by flame synthesis. **b.** The catalytic performance of CO conversion as a function of temperature. Reproduced with permission.[167] Copyright 2020, Elsevier Inc. **c.** The mechanism illustration for CNTs as microwave antennas in photocatalysis. **d.** UV-light-driven photocatalytic NO oxidation performances. Reproduced with permission.[168] Copyright 2019, Springer Nature. **e.** The experimental procedures for synthesizing MXene, MXene-NH_2, and MXene-PIL. **f.** Adsorptive removal of iodine on MXene, MXene-NH_2 and MXene-PIL. Reproduced with permission.[169] Copyright 2021, Elsevier Inc. **g.** schematic of turning plastic bag into graphene powder through flash joule heating. **h.** Raman spectra of the alternating current flash graphene, direct current turbostratic flash graphene and commercial graphene. Reproduced with permission.[170] Copyright 2020, American Chemical Society.

Pollution issues include gas, liquid, and solid waste, where ultrafast synthesis/manufacturing assisted techniques could play an important role in materials development and technological advancement. For example, SACs are of great interest in many catalytic reactions, including gas treatment, while high-temperature stability remains a challenge. Taking advantage of the high reaction temperature in flame pyrolysis synthesis, Yan et al. prepared high-temperature-stable Pt SAC on several oxide supports (Al_2O_3, SiO_2, TiO_2 and ZrO_2, **Fig. 10a**), among which ZrO_2 supported Pt SAC shows the best stability and most substantial catalytic effect.[167] As exhibited in **Fig. 10b**, the CO conversion temperature of the pyrolysis synthesized $0.1Pt_1/ZrO_2$-flame was much lower than that for the wet chemical method. The result demonstrated that ultrafast flame pyrolysis could synthesize highly stable materials with improved CO elimination performance, benefiting applications such as automobile exhaust treatment. In another example, Chloroplast-like, non-continuously distributed semiconductors threaded by carbon nanotubes were synthesized using

microwave-assist method, leading to outstanding photocatalytic performance (**Fig. 10c**). The TiO_2 nanoparticles function as a photocatalytic center, while carbon nanotube provides a 3D fast electron transport pathway. This unique hierarchical structure achieves a record-breaking efficiency of 86% for NO removal (ultraviolet irradiation) with desirable stability (**Fig. 10d**).[168]

Water treatment with functional adsorbents is another crucial aspect for environmental recovery and protection. In recent years, the applications of MXene (a family of transition metal carbides or carbonitrides, M stands for transition metals, and X is usually C and/or N elements) based adsorbents have been widely studied.[171] However, their performances are still limited due to the scarcity of functional groups and adsorption sites. Ultrafast microwave-assisted synthesis offers a facile route for MXene polyimidazole (named as MXene-PIL) functionalization; the synthesis process is illustrated in **Fig. 10e**. The obtained adsorbent was synthesized through a microwave-irradiation-assisted multi-component reaction to remove iodine from water. As shown in **Fig. 10f**, compared to the adsorption curve of iodide with MXene and MXene-NH_2, the adsorption capacity of MXene-PIL is much higher.[169] This result offers an important material system for harmful nuclear waste (^{129}I) treatment, greatly benefiting humankind and our ecosystem.

Solid waste treatment is another important field of study for environmental protection. Particularly, unrecyclable plastic waste has been a pressing issue for both land and the ocean, endangering the health of ocean life, animals, and human beings. Tremendous efforts have been applied to reduce the amount of plastic waste through physical and chemical recycling. However, most current recycling technologies are still not cost-effective; only 9% of produced plastic waste has been recycled.[172,173] Facile, low-cost recycling technologies are urgently needed. Tour et al.[170] proposed a flash Joule heating method utilizing AC and DC that recycles plastic waste and turns it into higher-value graphene (**Fig. 10g**). Using this method, outstanding-quality turbostratic flash graphene with a high I_{2D}/I_G peak (from Raman spectroscopy) ratio (1~6) and low-intensity D band was fabricated, much better than that of commercial graphene, turning waste into treasure (**Fig. 10h**).
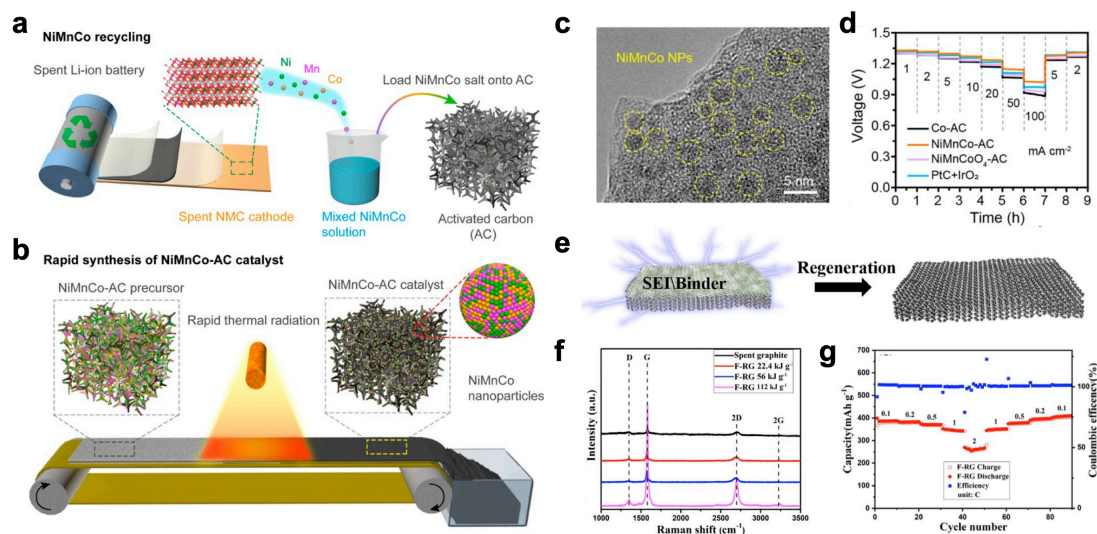
Fig. 11 Ultrafast synthesis for battery recycling. (a) Schematic of spent battery cathode materials separation/refining for (b) ultrafast thermal radiation synthesis of catalysts. (c) TEM image of NiMoCo nanoparticles/AC prepared through ultrafast synthesis and (d) rate performance of zinc-air batteries using NiMoCo-AC catalysts. Reproduced with permission.[174] Copyright 2022, CC BY-NC-ND 4.0 (e) schematic of ultrafast regeneration of spent graphite anode (f) Raman spectrum of spent graphite with various ultrafast treatment conditions (g) rate performance of regenerated spent graphite. Reproduced with permission.[175] Copyright 2022, CC BY 4.0

The soaring number of electrical vehicles and energy storage plants in the past decade indicate spent battery recycling will be a pressing issue in the near future.[176] The development of battery recycling technologies not only benefits the environment, but also turns waste elements into resources and wealth. Conventional spent battery electrode materials are usually recycled through pyrometallurgical or hydrometallurgical techniques, which are time/energy consuming.[177] Zhou et al. utilizes $LiNi_{1-x-y} Mn_x Co_y O_2$ cathode from spent battery (**Fig. 11a**) as source for bifunctional NiMnCo nanoparticle catalysts with ultrafast radiative synthesis (**Fig. 11b**). As-synthesized particles can be uniformly loaded on activated carbon substrates (**Fig. 11c**), and the Zn-air batteries utilizing these catalysts demonstrate great rate performance even better than commercial PtC+IrO$_2$ catalysts (**Fig. 11d**).[174] Utilizing ultrafast flash joule heating, spent graphite anodes can also be regenerated (**Fig. 11e**) and healed (**Fig. 11f**), demonstrating excellent rate performance (**Fig. 11g**).[175]

Table.1 Summary of ultrafast synthesis methods

Methods	Structure	Materials	Time	Temperature(K)	Medium	Applications	Ref.
Joule Heating	0D	Metal	Milliseconds	~1700	Carbon paper	Li-air battery	178
	0D	Metal	Milliseconds	~1700	RGO matrix	Energetic Mater.	179
	0D	Metal	Seconds	~1601	Carbon black	EOR	180
	0D	Oxide	Seconds	~1438	Carbon cloth	Fuel cells	181
	0D	Carbide	Seconds	>3000	Graphene	HER	182
	1D	SiNWs	Milliseconds	~2100	RGO	Li-ion battery	25
	2D	Oxide	Minutes	~2936	CNTs	Al-ion battery	183
	2D	Sulfide	Milliseconds	—	Copper wool	HER	184
	2D	Graphene	Milliseconds	~3000	Quartz tube	Plastic	185
	3D	Oxide	Seconds	~2073	Carbon felt	Li-ion battery	186
Laser	0D	Metal	Femtoseconds	—	—	Microdevices	187
	2D	MXene	Femtoseconds	—	PET substrate	Supercapacitors	188
	2D	CNTs	Femtoseconds	—	Al substrate	Supercapacitors	189
	2D	Graphene	Microseconds	~1773	Cu foil	Na-ion battery	190
	3D	MOFs	Femtoseconds	~2273	Quartz	Supercapacitors	191
	3D	Halide	Femtoseconds	—	MAPbI$_3$ films	Solar Cells	192
Microwave	0D	Metal	Seconds	—	Graphene	HER	193
	0D	Metal	Seconds	—	Graphene	OER	148
	0D	Oxide	Minutes	—	Solution	Li-ion battery	194
	0D	Phosphide	Seconds	—	CNTs	Supercapacitors	195
	—	Organic	Seconds	>1273	—	Chemicals	196
	—	Organic	Seconds	~3000	—	Fuels	197
	2D	RGO	Seconds	1073	—	Na-ion battery	198
Flame	0D	Metal	—	—	TiO$_2$	NO$_X$ removal	199
	0D	Oxide	—	1350	—	Li-ion battery	200
	0D	Oxide	—	1500	—	NO$_X$ removal	201
	0D	Oxide	Milliseconds	748	—	Gas sensors	202
	0D	Oxide	—	—	—	Magnet	203
Plasma	0D	Oxide	Seconds	—	—	HER	204
	2D	Halide	Milliseconds	—	PEDOT:PSS	Solar cells	149
	2D	Graphene	Minutes	—	GO	Li-S battery	129
	3D	Nitride	Minutes	723	Carbon cloth	HER	127
Infrared	0D	Metal	Seconds	2873	PEN	Electronics	86
	2D	Oxide	Minutes	748	FTO	Solar cells	50
	2D	RGO	Minutes	—	—	Li-ion battery	94
Inductive heating	0D	Metal	Seconds	1773	Carbon paper	HER	205
	1D	CNTs	Minutes	1183	—	Sensors	206
	2D	Oxides	Minutes	387	Ni foam	HER	51
	2D	Graphene	Seconds	1423	Cu foil	Li-ion battery	207

3. Ultrafast Methods for Advanced Manufacturing

Besides high efficiency for rapid R&D and prototyping in research labs, ultrafast synthesis techniques are also highly suitable for mass production, partly because they generally involve fewer synthesis and solvent-washing steps. They are also compatible with roll-to-roll production and large reactors. Examples of typical scalable methods are introduced below, which are organized as the dimensionality of the manufactured products evolved from 0D to 3D.
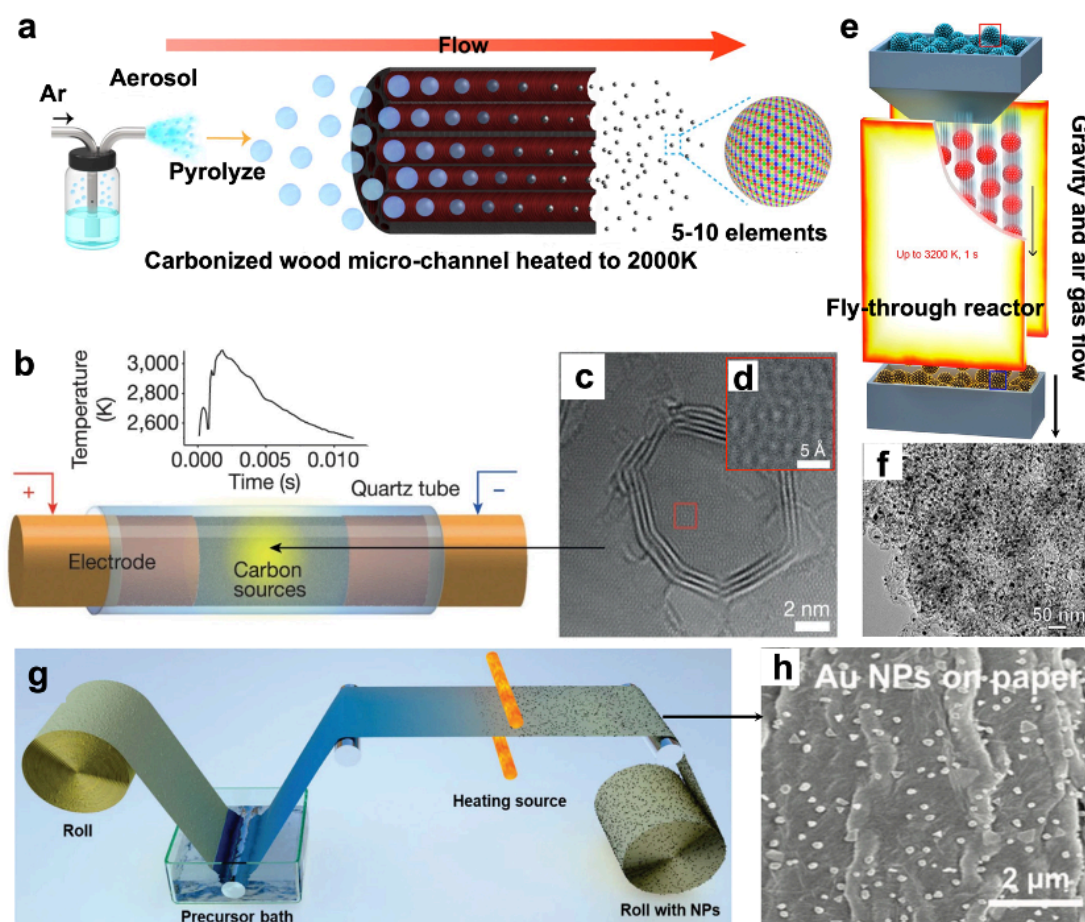

Fig. 12 Ultrafast methods for manufacturing 0D materials. a. Schematic of precursor droplets transporting through the high temperature (up to 2000K) carbonized wood microchannels for scalable nanoparticle synthesis. Reproduced with permission.[208] Copyright 2020, Elsevier Inc. b. Schematic of the flash Joule heating process and its temperature vs. time plot (inset). c-d. HR-TEM images of flash graphene from carbon black. Reproduced with permission.[185] Copyright 2020, Springer Nature. e. Schematic illustration of the fly-through high-temperature reactor with joule heating for metal-loaded carbon nanoparticles. f. TEM image of the Pt NP/C synthesized with the fly-through reactor. Reproduced with permission.[53] Copyright 2021, American Chemical Society. g. Schematic of roll-to-roll production of nanoparticles loaded on arbitrary substrate. h. SEM image of Au nanoparticles loaded on cellulose paper substrate via ultrafast radiative heating synthesis. Reproduced with permission.[209] Copyright 2019, Royal Society of Chemistry.

Hu et al. reported a "droplet-to-particle" aerosol continuous synthesis technique to

manufacture various types of nanoparticles.[204] As shown in **Fig. 12a**, precursor droplets containing homogeneously mixed metal salts travels through the microchannels of the carbonized wood reactor (carried with Argon carrier gas), where the precursor obtains a short stay and uniform heating. The excellent heating capability provides an ideal and efficient way for the continuous synthesis of nanomaterials, especially those that require relatively extreme processing conditions, such as high-entropy and high-entropy alloy/oxide (HEA/HEO) nanoparticles. The authors demonstrated that CrMnFeCoNi HEA nanoparticles could be continuously synthesized over 6 hours (5 L min^{-1} flow rate of Ar), and the production rate can reach up to 100 mg h^{-1} at the lab scale. With the flash joule heating method, gram-scale graphene can be made rapidly and scalably from inexpensive carbon sources (e.g., coal, biochar, carbon black, plastic, etc.) in a bottom-up manner (**Fig. 12b-d**). This process involves no solvent or harsh oxidants, which is economically and environmentally friendly. Besides carbon, functional particles such as carbon black loaded Pt nanocrystals can be made through a "fly-through" ultrafast synthesis method. As shown in **Fig. 12e**, the desired product can be rapidly produced when precursors pass through (with gravity or gas flow) joule heated carbon papers. The as-synthesized Pt/C (**Fig. 12f**) obtained an excellent methanol oxidation reaction activity, significantly better than commercial Pt/C under the same testing conditions. Other than metals and oxides, researchers also demonstrated ultrafast synthesis techniques for manufacturing carbides, in which a yield of 12g of SiC are produced with a surface area of 460 m^2 g^{-1}. Inspired by the highly efficient joule heating and IR radiative heating technologies, a rapid, efficient method enabling the roll-to-roll preparation of nanoparticles on arbitrary substrates (especially temperature-sensitive ones) was reported (**Fig. 12g**). Well-dispersed nanoparticles such as Pt, Au, and Ru can be generated on paper or textile substrate under radiative heating (**Fig. 12h**). The substrate can move across a 2000 K heating source at a continuous production speed of 0.5 cm s^{-1}. These techniques demonstrate the possibility of ultrafast manufacturing functional materials on soft substrates, which could play an essential role in personal thermal management, medical, and wearable applications.
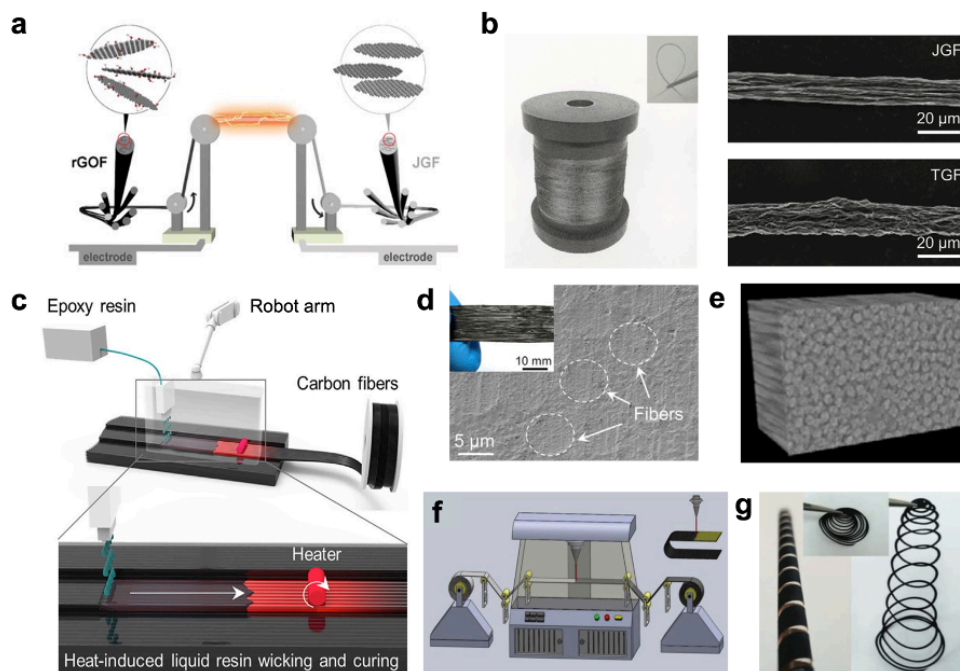
Fig. 13 Ultrafast methods for manufacturing 1D materials. a. Schematic of the Joule heating system. b. Schematic showing the conformational change of the graphene sheets. Reproduced with permission.[210] Copyright 2021, John Wiley & Sons, Inc. c. Schematic of localized in-plane thermal assisted (LITA) 3D printing approach. d. The all-in-one design of the printing head. e. CT reconstructed cross-sectional images of the composites. Reproduced with permission.[211] Copyright 2020, Elsevier Inc. f. Schematic illustration of LIGP fabrication. g. Demonstrations of LIGP with various strimmed shapes. Reproduced with permission.[212] Copyright 2018, John Wiley & Sons, Inc.

Manufacturing one-dimensional (1D) fiber materials with light weight, high mechanical strength, and other specific functions is of significant research and industrial interest globally. Liu et al. reported the utilization of the Joule heating method that converted defective graphene oxide (GO) fibers into highly crystalline graphene fibers in a scalable fashion (**Fig. 13a and b**).[210] This method enables ultrafast high-temperature (at ~2000°C) treatment and low energy consumption (~2000 kJ m^{-1}), which is highly efficient in producing continuous graphene fibers. Compared with thermally annealed graphene fibers without applied current, the graphene fibers synthesized by a dynamic joule heating system have enhanced electrical and mechanical strength. Another example reported by Fu et al. demonstrates the printing of continuous carbon fiber composite via IR radiative heating, as illustrated in **Fig. 13c**.[211] The integrated print-head design consists of a liquid resin nozzle, carbon nanotube heater, guide rod, and carbon fiber spool, where the heating solidifies the liquid polymer in a carbon fiber structure. The printed composite are with aligned structure (**Fig. 13d and e**), high fiber volume fraction (58.6%), and degree of curing (95%), which lead to high mechanical strength (810 MPa) and modulus (108 GPa). Scalable graphene fiber and paper can also be made through laser-induced fabrication (**Fig. 13f** and **g**).[212] The graphene paper can be further processed into complex shapes for stretchable electronics applications when

alternating laser power. By adjusting the laser power and other processing parameters, the production rate of the laser-induced graphene paper can reach as high as 30 cm^2 min^{-1} at the lab scale. These inventions paved the way for the quick and continuous manufacturing of 1D materials with high efficiency and massive productivity.

Besides 1D structured materials, ultrafast methods can also be used for 2D (surface, thin film) manufacturing. Similar to Liu et al. in **Fig. 13a**, Gao et al. independently developed a scalable, roll-to-roll joule hearing technique that converts reduced graphene oxide films into highly electrically and thermally conductive films.[213] As-fabricated graphene films can achieve an outstanding electrical conductivity of 4.2×10^5 S m^{-1} and thermal conductivity of ~1285 W mK^{-1}, making them useful in thermal management, flexible electronics, and wearable devices.
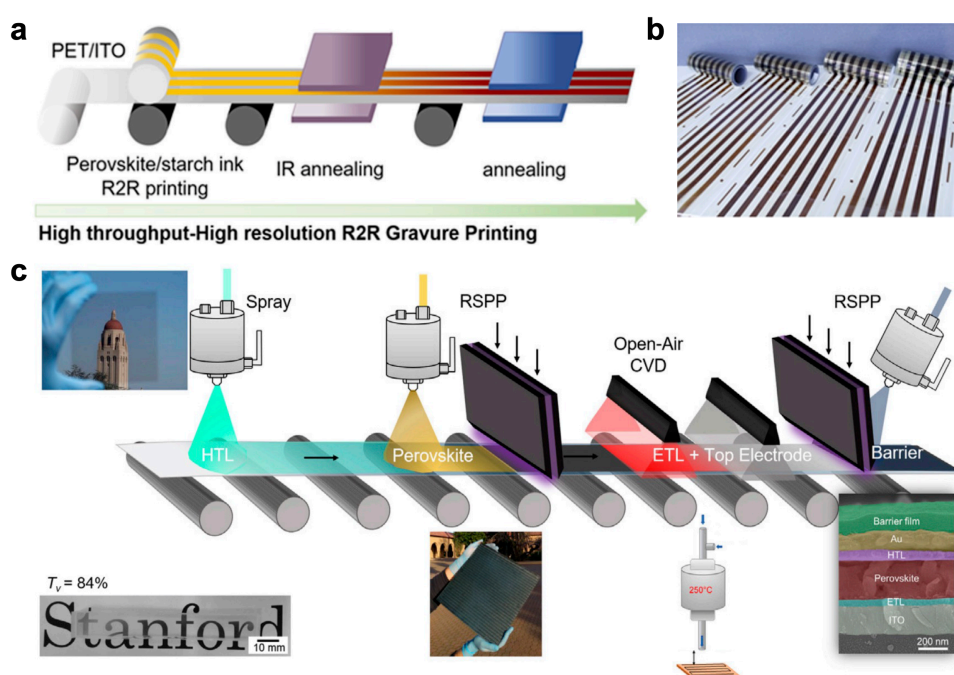

Fig. 14 Ultrafast methods for 2D manufacturing. a. Infrared technique for the roll-to-roll printing process of the as-developed perovskite/starch inks. b. Plasma technique for the schematic of high-throughput open-air production for in-line, fast, and scalable manufacturing of perovskite solar modules. Reproduced with permission.[214] Copyright 2021, Elsevier Inc. c. Schematic of high-throughput open-air production for in-line, fast and scalable manufacturing of perovskite solar modules. Reproduced with permission.[215] Copyright 2021, CC BY 4.0.

A specific area of interest for thin film manufacturing is photovoltaics (PV), which perovskite solar cells are of particular enthusiasm for their soaring power conversion efficiency (PCE) and optimistic industrial potential. However, most of the perovskite solar cells with high PCE are fabricated at a lab scale with extreme control of environmental conditions, which is challenging for scalable production. Anti-solvent bath is proven to be effective for roll-to-roll fabrication, but it is a relatively complex process, rendering increased manufacturing costs and waste disposal problems. To

alleviate this issue, Rizzo et al.[214] demonstrated a starch polymer-modified perovskite precursor with an infrared radiation-assisted roll-to-roll fabrication process (**Fig. 14a**) to avoid the anti-solvent bath step. A 50-meter-long printed PET roll with a printing speed of up to 3.0 m min^{-1} is demonstrated with their pilot line. The manufactured device achieved an impressive PCE higher than 10% (**Fig. 14b**). More intriguingly, Dauskardt et al. reported a rapid plasma processing method that not only covered most of the key materials' fabrication in perovskite solar cells (**Fig. 14c**) and obtained the highest PCE at the time but also achieved reproducibility, moisture immunity of device fabrication in open-air.[215] With the open-air plasma treatment, continuous, in-line processing at 12 m min^{-1} without any post-anneal can be achieved for solar cell fabrication. Critically, the above mention methods are highly efficient and tunable, allowing the utilization of flexible and thermally sensitive substrates, paving the way for developing commercially viable next-generation thin-film PV technologies.
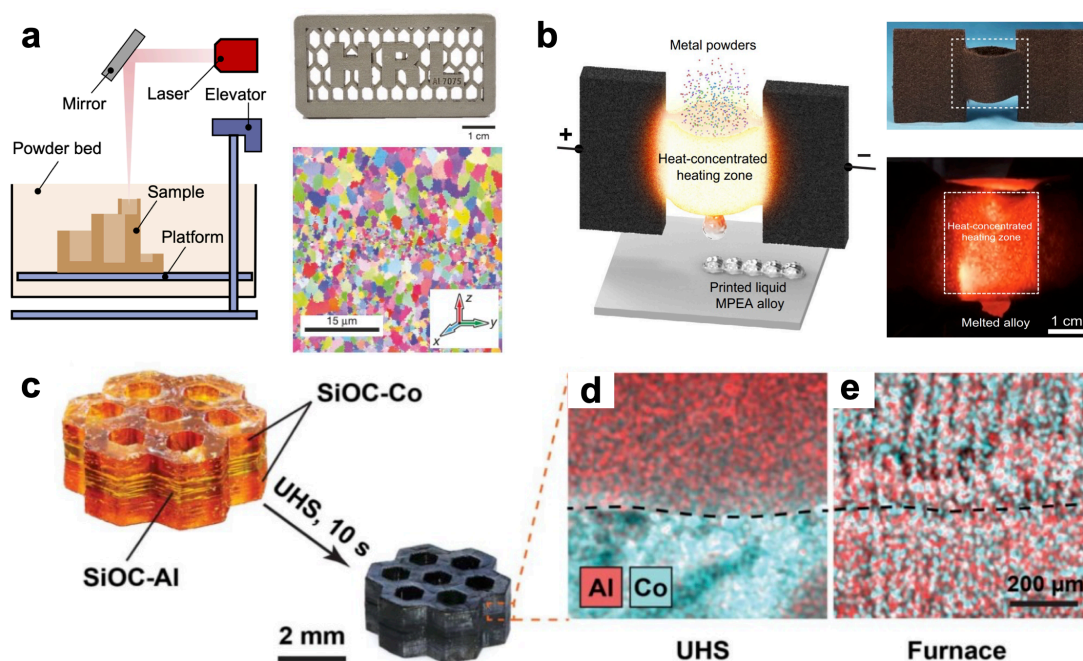

Fig. 15 Ultrafast methods for 3D manufacturing. a. laser-assisted methods for additive manufacturing. Reproduced with permission.[216] Copyright 2017, Springer Nature. b. The ultrahigh-temperature melting platform for MPEAs additive manufacturing. Reproduced with permission.[217] Copyright 2017, Springer Nature. c. Ultrafast sintering of 3D structured materials with heterojunction and d. EDS mapping at the heterojunction. e. EDS mapping at the heterojunction of furnace sintered material. Reproduced with permission.[31] Copyright 2020, The American Association for the Advancement of Science.

The high energy, high power, and ultrafast features enable unique structure and property of as fabricated products, which can also be extended to 3D structured bulk materials. A typical example is the widely utilized laser-assisted additive manufacturing. (**Fig. 15a**) Although laser-assisted techniques can rapidly melt precursor power, the equivalently fast solidification usually lead to large columnar

grains and crack formation in the final product, hindering metal-based additive manufacturing to unleash its full potential.[216] To address this issue, Pollock et al. proposed an effective method with precursor engineering. They designed lattice-matching nanoparticle-enhanced precursor powder that allows uniform nucleation and equiaxed crystal growth at solidification (**Fig. 15a** right corner). This method is demonstrated effective in printing high-strength aluminum alloys, which is also believed to be generalized to a broad range of alloys. Moreover, Hu et al. successfully prepared multi-principal element alloys (MPEA, with a feeding rate of 300 mg min^{-1}) utilizing the rapid melting and solidification characteristic of ultrafast methods since rapid cooling limits the diffusion process to avoid segregation (**Fig. 15b**).[217] For the same reason, the ultrafast synthesis method allows the sintering of 3D-printed ceramics (**Fig. 15c**) with sharp compositional heterojunctions (**Fig. 15d**).[31] In contrast, materials fabricated with a furnace has blurry boundary due to prolonged diffusion time (**Fig. 15e**). The above examples showcase the uniqueness of ultrafast synthesis techniques in the advanced manufacturing of functional materials and structures.

Table. 2 Comparison of gas atmosphere, energy consumption, and energy utilization for different synthesis methods.

Methods	Materials	Gas Atmosphere	Energy Consumption (kJ h^{-1})	Energy Efficiency	Ref.
Furnace Annealing	GFs	Air	10^4~10^5	50%-80%	213
Joule Heating	GFs	Ar	10^3~10^4	>90%	213
	Alloy/Oxide	Ar			208
	Graphene	Vacuum			185
Laser	LIGP	Ar	10~10^2	50%~60%	212
Inductive Heating	CNTs	Vacuum	10^3~10^4	>90%	206
Infrared	r-GO films	Air/N$_2$	10^2~10^3	>90%	94
	Ag layers	Air			86

4. Perspectives and Conclusions

One of the bottlenecks for technological advancement in energy and the environment lies in materials development and discovery. Ultrafast synthesis techniques can overcome such limitations with a rich materials library, outstanding synthesis controllability, excellent materials quality, and superior scalability. Remarkably, ultrafast synthesis techniques are straightforward and efficient to implement, significantly improving the efficiency of experiments. Furthermore, they also provide more room for researchers in developing advanced technologies.

Despite the great success of ultrafast synthesis methods, there are drawbacks that are yet to be overcome. For the preparation of nanomaterials, when compared with conventional wet chemical synthesis methods, the tunability of ultrafast techniques is less versatile. Nanoparticles with selected crystal planes, complex nanostructured materials such as Janus[218] or heterostructured nanoparticles,[219] hierarchically structured materials[220] are still rarely reported. In addition, surface functionalization of nanomaterials with surfactants is less common with the ultrafast synthesis methods, as instantaneous high energy could quickly destroy somewhat fragile surfactants. However, surface functionalization could be vitally important to materials processing (solution-based process) and their performance in applications.[221] In addition, the future production of kilograms or even tons of complex structured nanomaterials with ultrafast manufacturing methods remains a challenge, even though grams-quantity samples have already been demonstrated in research labs.

The rapid heating of ultrafast synthesis methods is advantageous for nanomaterials synthesis but may be a limitation for bulk materials. This can be particularly true for complex structured materials (3D printed complex structured materials), where heat can be difficult to be accessed uniformly in precursor materials. Heat transfer during the heating/cooling process of ultrafast synthesis should be studied in detail to make desired materials with low surface-to-volume ratio (e.g. bulk materials). Microwave-assisted techniques may partially overcome this problem, as microwave can be well-absorbed throughout a material. On the other hand, this heating/cooling provides a unique degree of freedom in new materials design. For example, temperature gradients could be designed in the materials synthesis process, leading to desirable chemical/electrical/mechanical gradient materials that cannot be synthesized with other techniques. In addition, the heating rate can be adjusted/programmed by tuning the energy input, which can significantly affect the microstructure of materials, leading to distinctive properties of synthesis products. However, the cooling rate of materials with low surface-to-volume ratio may still be a limitation, especially when metastable phases are desired.
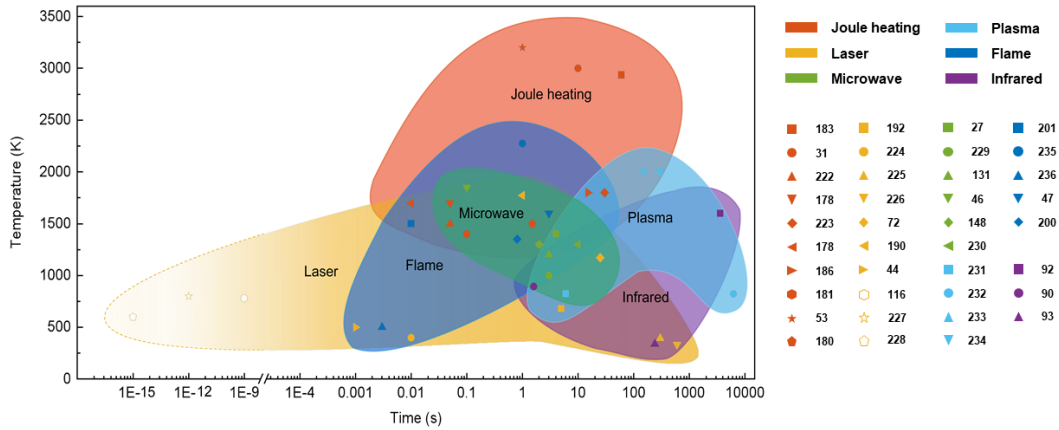
Fig. 16 Diagram of synthesis conditions of ultrafast methods: temperature vs. reaction time

The precise control of materials synthesis with ultrafast synthesis techniques, both temporally (ps, fs) and spatially (nm, atomic), can be further improved.[66,237-239] The majority of reported ultrafast syntheses have synthesis times in the range of microseconds to a few minutes, as shown in **Fig. 16**. Studies into more precise time control (meanwhile tuning reaction temperature) in various ultrafast synthesis techniques, such as laser-assisted methods, could lead to a better synthesis heating/cooling rate. Ultrafast synthesis techniques also have not demonstrated high-resolution (sub-nm) spatially resolved materials, yet they are possible and highly desired in applications such as catalysis.[240-242] A versatile choice of materials can be synthesized with future highly spatial and temporal resolved ultrafast synthesis techniques. The scalable production (in kilograms or tons) of highly precise materials (in terms of microstructures and resolutions) is also challenging but of vital importance to a broader application of ultrafast manufacturing.[243-245]
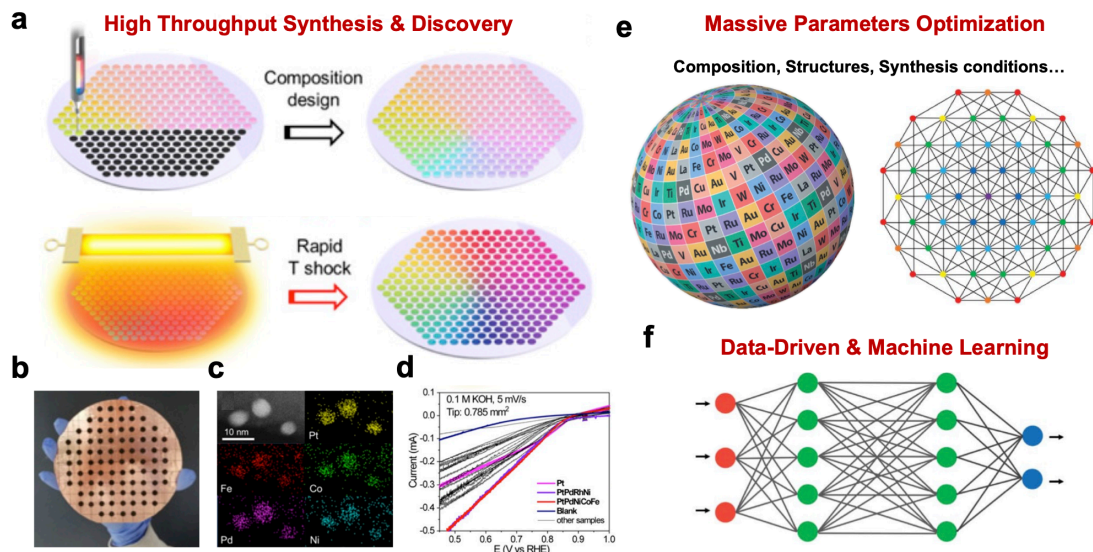

Fig. 17 High-throughput and data-driven materials discovery with ultrafast methods. (a) schematic of high throughput materials synthesis and discovery with ultrafast radiative synthesis of catalysts; (b) photo image of patterned sample on Cu substrate; (c) TEM image and elemental maps of

PtPdFeCoNi nanoparticles; (d) fast screening of multimetallic ORR catalysts. Reproduced with permission.[246] Copyright 2020，CC BY-NC-ND 4.0. (e) schematic illustrate the massive parameter space for materials discovery for energy and environment applications; (f) Data-driven materials discovery with ultrafast methods and neuron networks. Reproduced with permission.[247] Copyright 2022，The American Association for the Advancement of Science.

Tremendous challenges and opportunities lie in further developing ultrafast synthesis technologies for advanced materials development. Modifications to the abovementioned ultrafast synthesis methods, combining ultrafast synthesis with conventional wet chemical synthesis, can be developed in addressing the challenges above. To better use ultrafast synthesis methods, high-throughput and advanced characterization techniques should also be developed for an overall efficient R&D process in technological advancement. As illustrated in **Fig. 17a-d**, multielement metallic nanoparticle catalysts can be prepared and tested in a high-throughput fashion.[246] It can be further combined with machine learning algorithms for accelerated data-driven materials discovery (**Fig. 17e and f**).[247]

Despite the excitement, ultrafast synthesis methods are still in their infancy. As we are encountering pressing global challenges from the energy crisis, environment/water contamination, food shortage, and health care issues, solutions are urgently needed. Fortunately, ultrafast synthesis methods may offer facile and highly efficient solutions for tackling materials R&D for nearly all the above challenges. We anticipate the adoption of ultrafast synthesis and manufacturing techniques for technologies far beyond energy and the environment (**Fig. 18**), where abundant opportunities lie in this exciting area of study.
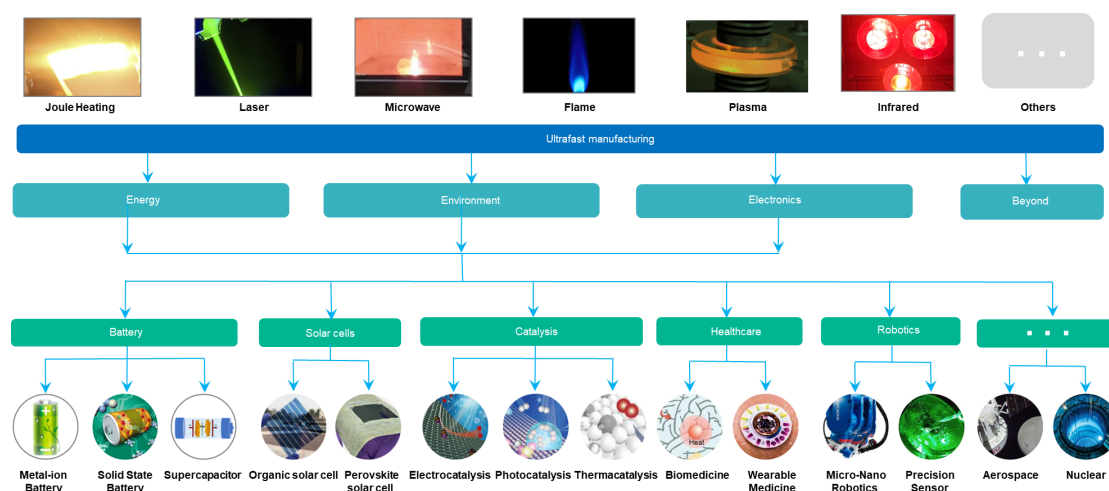

Fig. 18 Ultrafast manufacturing for future applications. Reproduced with permission.[178] Copyright 2019, Elsevier Ltd. Reproduced with permission.[248] Copyright 2021, Springer Nature. Reproduced with permission.[27] Copyright 2019, John Wiley & Sons, Inc. Reproduced with permission.[80] Copyright 2021, Springer Nature. Reproduced with permission[36] Copyright 2018, American Chemical Society. Reproduced with permission[90] Copyright 2019, Elsevier Ltd. Reproduced with permission.[249] Copyright 2013, American Chemical Society. Reproduced with permission.[250] Copyright 2017,

References

1. J. H. Williams, A. DeBenedictis, R. Ghanadan, A. Mahone, J. Moore, W. R. Morrow, S. Price and M. S. Torn, *Science*, 2012, **335**, 53-59.

2. F. Schreyer, G. Luderer, R. Rodrigues, R. C. Pietzcker, L. Baumstark, M. Sugiyama, R. J. Brecha and F. Ueckerdt, *Environ. Res. Lett.*, 2020, **15**, 114016.

3. Y. Li and Q. Cui, *Appl. Energ.*, 2017, **199**, 13-24.

4. J. Jiang, B. Ye and J. Liu, *Appl. Energ.*, 2019, **235**, 186-203.

5. Y. B. Attahiru, M. M. A. Aziz, K. A. Kassim, S. Shahid, W. A. Wan Abu Bakar, T. F. Nsashruddin, F. A. Rahman and M. I. Ahamed, *Renew. Sust. Energ. Rev.*, 2019, **101**, 600-613.

6. H. Yang, I. Shahzadi and M. Hussain, *J. Environ. Manage*, 2021, **298**, 113385.

7. L. Tozer and N. Klenk, *Energy Res. Soc. Sci.*, 2018, **35**, 174-181.

8. A. Sikora, *ERA Forum*, 2020, **21**, 681-697.

9. M. Ossewaarde and R. Ossewaarde-Lowtoo, *Sustainability*, 2020, **12**, 9825.

10. K. Dahal and J. Niemelä, *Climate*, 2016, **4**, 36.

11. W. Du, Q. Huang and S. Grasso, *E3S Web of Conferences*, 2021, **308**, 01021.

12. S. Fujimori, K. Oshiro, H. Shiraki and T. Hasegawa, *Nat. Commun.*, 2019, **10**, 4737.

13. S. Song, H. Lin, P. Sherman, X. Yang, C. P. Nielsen, X. Chen and M. B. McElroy, *Nat. Commun.*, 2021, **12**, 6953.

14. M. Sugiyama, S. Fujimori, K. Wada and J. Weyant, *Sustain. Sci.*, 2021, **16**, 347-353.

15. Y. Tsunetsugu and M. Tonosaki, *J. Wood Sci.*, 2010, **56**, 339-344.

16. M. Vaka, R. Walvekar, A. K. Rasheed and M. Khalid, *J. Clean. Prod.*, 2020, **273**, 122834.

17. A. Watabe, J. Leaver, H. Ishida and E. Shafiei, *Energ. Policy*, 2019, **130**, 227-242.

18. Y. Zhang, S. Guo, X. Shi, X. Qian and R. Nie, *Appl. Energ.*, 2021, **299**, 117338.

19. Y. Yu and N. Zhang, *Energy Econ.*, 2021, **96**, 105125.

20. C. Xu, J. Yang, L. He, W. Wei, Y. Yang, X. Yin, W. Yang and A. Lin, *Environ. Dev.*, 2021, **37**, 100608.

21. R. Wang, Q. Wang and S. Yao, *J. Environ. Manage*, 2021, **293**, 112958.

22. B. Jung, J. Park, D. Seo and N. Park, *ACS Sustain. Chem. Eng.*, 2016, **4**, 4079-4083.

23. Y. K. Jeong, S. H. Park and J. W. Choi, *ACS Appl. Mater. Inter.*, 2018, **10**, 7562-7573.

24. Z. Yu and J. Thomas, *Adv. Mater.*, 2014, **26**, 4279-4285.

25. J. Lu, S. Liu, J. Liu, G. Qian, D. Wang, X. Gong, Y. Deng, Y. Chen and Z. Wang, *Adv. Energy Mater.*, 2021, **11**, 2102103.

26. Y. Deng, Z. Ni, A. F. Palmstrom, J. Zhao, S. Xu, C. H. Van Brackle, X. Xiao, K. Zhu and J. Huang, *Joule*, 2020, **4**, 1949-1960.

27. G. Zhong, S. Xu, C. Chen, D. J. Kline, M. Giroux, Y. Pei, M. Jiao, D. Liu, R. Mi, H. Xie, B. Yang, C. Wang, M. R. Zachariah and L. Hu, *Adv. Funct. Mater.*, 2019, **29**, 1904282.

28. F. Schneider, S. Suleiman, J. Menser, E. Borukhovich, I. Wlokas, A. Kempf, H. Wiggers and C. Schulz, *Rev. Sci. Instrum.*, 2019, **90**, 085108.

29. Z. Mao, J. Chen, Y. Yang, L. Bie, B. D. Fahlman and D. Wang, *Carbon*, 2017, **123**, 651-659.

30. C. D. Marco, S. M. Eaton, R. Suriano, S. Turri, M. Levi, R. Ramponi, G. Cerullo and R. Osellame, *ACS Appl Mater Inter.*, 2010, **2**, 2377-2384.

31. C. Wang, W. Ping, Q. Bai, H. Cui, R. Hensleigh, R. Wang, A. H. Brozena, Z. Xu, J. Dai, Y. Pei, C. Zheng, G. Pastel, J. Gao, X. Wang, H. Wang, J.-C. Zhao, B. Yang, X. R. Zheng, J. Luo, Y. Mo, B. Dunn and L. Hu, *Science*, 2020, **368**, 521–526

32. J.-Y. Song, C. Kim, M. Kim, K. M. Cho, I. Gereige, W.-B. Jung, H. Jeong and H.-T. Jung, *Sci. Adv.*, 2021, **7**, eabk2984.

33. Z. Lin, X. Zhao, C. Wang, Q. Dong, J. Qian, G. Zhang, A. H. Brozena, X. Wang, S. He, W. Ping, G. Chen, Y. Pei, C. Zheng, B. C. Clifford, M. Hong, Y. Wu, B. Yang, J. Luo, P. Albertus and L. Hu, *Small*, 2022, **18**, e2107951.

34. S. Pan, C. Liu, Y. Li, C. Wang, X. Cui, N. Liu, C. Zhang, I. Hakizimana, X. Zhao, W. Liu and Y. Chen, *Electrochim. Acta*, 2022, **433**, 141262.

35. W. Zhu, J. Zhang, J. Luo, C. Zeng, H. Su, J. Zhang, R. Liu, E. Hu, Y. Liu, W. D. Liu, Y. Chen, W. Hu and Y. Xu, *Adv. Mater.*, 2022, DOI: 10.1002/adma.202208974, e2208974.

36. Z. Wang, Y. Zhang, E. C. Neyts, X. Cao, X. Zhang, B. W. L. Jang and C. Liu, *ACS Catal.*, 2018, **8**, 2093-2110.

37. Q. Dong, M. Hong, J. Gao, T. Li, M. Cui, S. Li, H. Qiao, A. H. Brozena, Y. Yao, X. Wang, G. Chen, J. Luo and L. Hu, *Small*, 2022, **18**, e2104761.

38. L. Lai, J. Li, Y. Deng, Z. Yu, L. Wei and Y. Chen, *Small Structures*, 2022, **3**, 2200112.

39. C. Gu, H. M. Xu, S. K. Han, M. R. Gao and S. H. Yu, *Chem. Soc. Rev.*, 2021, **50**, 6671-6683.

40. H. Huang, Y. Wu, J. He, H. Wang, X. Liu, K. An, W. Wu and Z. Lu, *Adv. Mater.*, 2017, **29**, 1701678.

41. K. Li and W. Chen, *Mater. Today Energy*, 2021, **20**, 100638.

42. W. Shi, H. Liu, Z. Li, C. Li, J. Zhou, Y. Yuan, F. Jiang, K. Fu and Y. Yao, *SusMat.*, 2022, **2**, 186-196.

43. Y. Yao, Z. Huang, P. Xie, S. D. Lacey, R. J. Jacob, H. Xie, F. Chen, A. Nie, T. Pu, M. Rehwoldt, D. Yu, M. R. Zachariah, C. Wang, R. Shahbazian-Yassar, J. Li and L. Hu, *Science*, 2018, **359**, 1489-1494.

44. R. Li, S. Yuan, W. Zhang, H. Zheng, W. Zhu, B. Li, M. Zhou, A. Wing-Keung Law and K. Zhou, *ACS Appl. Mater. Inter.*, 2019, **11**, 40564-40574.

45. Y. Peng, J. Cao, Y. Sha, W. Yang, L. Li and Z. Liu, *Light: Sci. Appl.*, 2021, **10**, 168.

46. H. Qiao, M. T. Saray, X. Wang, S. Xu, G. Chen, Z. Huang, C. Chen, G. Zhong, Q. Dong, M. Hong, H. Xie, R. Shahbazian-Yassar and L. Hu, *ACS Nano*, 2021, **15**, 14928-14937.

47. G. D. Zhang, Z. H. Wu, Q. Q. Xia, Y. X. Qu, H. T. Pan, W. J. Hu, L. Zhao, K. Cao, E. Y. Chen, Z. Yuan, J. F. Gao, Y. W. Mai and L. C. Tang, *ACS Appl. Mater. Inter.*, 2021, **13**, 23161-23172.

48. H. Kim, G. Lee, S. Becker, J.-S. Kim, H. Kim and B. Hwang, *J. Mater. Chem. C*, 2018, **6**, 9394-9398.

49. L. A. Castriotta, F. Matteocci, L. Vesce, L. Cina, A. Agresti, S. Pescetelli, A. Ronconi, M. Loffler, M. M. Stylianakis, F. Di Giacomo, P. Mariani, M. Stefanelli, E. M. Speller, A. Alfano, B. Paci, A. Generosi, F. Di Fonzo, A. Petrozza, B. Rellinghaus, E. Kymakis and A. Di Carlo, *ACS Appl. Mater. Inter.*, 2021, **13**, 11741-11754.

50. S. Sánchez, X. Hua, A. Günzler, Esteban Bermúdez-Ureña, D. Septiadi, M. Saliba and U. Steiner, *Cryst. Growth Des.*, 2020, **20**, 670−679.

51. G. Xiong, Y. Chen, Z. Zhou, F. Liu, X. Liu, L. Yang, Q. Liu, Y. Sang, H. Liu, X. Zhang, J. Jia and W. Zhou, *Adv. Funct. Mater.*, 2021, **31**, 2009580.

52. Q. Dong, Y. Yao, S. Cheng, K. Alexopoulos, J. Gao, S. Srinivas, Y. Wang, Y. Pei, C. Zheng, A. H. Brozena, H. Zhao, X. Wang, H. E. Toraman, B. Yang, I. G. Kevrekidis, Y. Ju, D. G. Vlachos, D. Liu and L. Hu, *Nature*, 2022, **605**, 470-476.

53. Y. Qiao, C. Chen, Y. Liu, Y. Liu, Q. Dong, Y. Yao, X. Wang, Y. Shao, C. Wang and L. Hu, *Nano Lett.*, 2021, **21**, 4517−4523.

54. T. Li, Q. Dong, Z. Huang, L. Wu, Y. Yao, J. Gao, X. Wang, H. Zhang, D. Wang, T. Li, R. Shahbazian-Yassar and L. Hu, *Adv. Mater.*, 2021, **34**, e2106436.

55. C. Li, Z. Wang, M. Liu, E. Wang, B. Wang, L. Xu, K. Jiang, S. Fan, Y. Sun, J. Li and K. Liu, *Nat. Commun.*, 2022, **13**, 3338.

56. B. Huang, M. Wang, C. Wu and L. Guan, *CCS Chemistry*, 2021, DOI: 10.31635/ccschem.021.202101353, 3473-3484.

57. Y. Yao, Z. Huang, P. Xie, L. Wu, L. Ma, T. Li, Z. Pang, M. Jiao, Z. Liang, J. Gao, Y. He, D. J. Kline, M. R. Zachariah, C. Wang, J. Lu, T. Wu, T. Li, C. Wang, R. Shahbazian-Yassar and L. Hu, *Nat. Nanotechnol.*, 2019, **14**, 851-857.

58. M. Cui, C. Yang, S. Hwang, M. Yang, S. Overa, Q. Dong, Y. Yao, A. H. Brozena, D. A. Cullen, M. Chi, T. F. Blum, D. Morris, Z. Finfrock, X. Wang, P. Zhang, V. G. Goncharov, X. Guo, J. Luo, Y. Mo, F. Jiao and L. Hu, *Sci. Adv.*, 2022, **8**, eabm4322.

59. Y. Chen, K. Fu, S. Zhu, W. Luo, Y. Wang, Y. Li, E. Hitz, Y. Yao, J. Dai, J. Wan, V. A. Danner, T. Li and L. Hu, *Nano Lett.*, 2016, **16**, 3616-3623.

60. W. Cai, J. Wang, P. Jiang, L. Cao, G. Mi and Q. Zhou, *J. Manuf. Syst.*, 2020, **57**, 1-18.

61. J. Lin, Z. Peng, Y. Liu, F. Ruiz-Zepeda, R. Ye, E. L. Samuel, M. J. Yacaman, B. I. Yakobson and J. M. Tour, *Nat. Commun.*, 2014, **5**, 5714.

62. A. Kanyilmaz, *Engineering Structures*, 2019, **183**, 1027-1048.

63. S. Marimuthu, J. Dunleavey, Y. Liu, B. Smith, A. Kiely and M. Antar, *J.Mater. Process. Techn.*, 2019, **271**, 554-567.

64. M. Malinauskas, A. Zukauskas, S. Hasegawa, Y. Hayasaki, V. Mizeikis, R. Buividas and S. Juodkazis, *Light: Sci. Appl.*, 2016, **5**, e16133.

65. G. Bansal, D. Bandhu Singh, H. Singh Virk, A. Devrani and A. Bhandari, *Mater. Today: Proceedings*, 2020, **26**, 833-837.

66. H. Zeng, X.-W. Du, S. C. Singh, S. A. Kulinich, S. Yang, J. He and W. Cai, *Adv. Funct. Mater.*, 2012, **22**, 1333-1353.

67. G. Mincuzzi, A. L. Palma, A. D. Carlo and ThomasM.Brown, *ChemElectroChem.*, 2016, **3**, 9-30.

68. W. Chen, R. V. Salvatierra, M. Ren, J. Chen, M. G. Stanford and J. M. Tour, *Adv. Mater.*, 2020, **32**, 2002850.

69. C. H. Dreimol, H. Guo, M. Ritter, T. Keplinger, Y. Ding, R. Gunther, E. Poloni, I. Burgert and G. Panzarasa, *Nat. Commun.*, 2022, **13**, 3680.

70. X. Liu, C. Xing, F. Yang, Z. Liu, Y. Wang, T. Dong, L. Zhao, H. Liu and W. Zhou, *Adv. Energy Mater.*, 2022, DOI: 10.1002/aenm.202201009, 2201009.

71. H. Yuan, L. Zhao, B. Chang, Y. Chen, T. Dong, J. He, D. Jiang, W. Yu, H. Liu and W. Zhou, *Appl. Catal. B: Environmen.*, 2022, **314**, 121455.

72. R. Ye, D. K. James and J. M. Tour, *Adv. Mater.*, 2019, **31**, 1803621.

73. Y. Lian, B. Han, D. Liu, Y. Wang, H. Zhao, P. Xu, X. Han and Y. Du, *Nano-Micro Lett.*, 2020, **12**, 153.

74. C.-L. Sun, C.-T. Chang, H.-H. Lee, J. Zhou, J. Wang, T.-K. Sham and W.-F. Pong, *ACS Nano*, 2011, **5**, 7788–7795.

75. J. Hu, A. Liu, H. Jin, D. Ma, D. Yin, P. Ling, S. Wang, Z. Lin and J. Wang, *J. Am. Chem. Soc.*, 2015, **137**, 11004-11010.

76. S. Chen, L. Nie, X. Hu, Y. Zhang, Y. Zhang, Y. Yu and W. Liu, *Adv Mater*, 2022, DOI: 10.1002/adma.202200430, e2200430.

77. Q. Chen, T. Ma, F. Wang, Y. Liu, S. Liu, J. Wang, Z. Cheng, Q. Chang, R. Yang, W. Huang, L. Wang, T. Qin and W. Huang, *Adv. Sci.*, 2020, **7**, 2000480.

78. F. Xu, Y. Zhou, X. Zhai, H. Zhang, H. Liu, E. H. Ang, Y. Lu, Z. Nie, M. Zhou and J. Zhu, *Small Methods*, 2022, **6**, e2101212.

79. R. Daiyan, E. C. Lovell, B. Huang, M. Zubair, J. Leverett, Q. Zhang, S. Lim, J. Horlyck, J. Tang, X. Lu, K. Kalantar-Zadeh, J. N. Hart, N. M. Bedford and R. Amal, *Adv. Energy Mater.*, 2020, **10**, 2001381.

80. J. Yu, X. Sun, X. Tong, J. Zhang, J. Li, S. Li, Y. Liu, N. Tsubaki, T. Abe and J. Sun, *Nat. Commun.*, 2021, **12**, 7209.

81. D. S. Jung, Y. N. Ko, Y. C. Kang and S. B. Park, *Adv. Powder Technol.*, 2014, **25**, 18-31.

82. Guojun Chen, Z. Chen, Z. Wang, R. Obenchain, D. Wen, H. Li, R. E. Wirz and Z. Gu, *Sci. Adv.* , 2021, **7**, eabg5686.

83. G. Chen, Z. Chen, D. Wen, Z. Wang, H. Li, Y. Zeng, G. Dotti, R. E. Wirz and Z. Gu, *Proc. Natl. Acad. Sci. USA*, 2020, **117**, 3687-3692.

84. D. Rupp, L. Fluckiger, M. Adolph, A. Colombo, T. Gorkhover, M. Harmand, M. Krikunova, J. P. Muller, T. Oelze, Y. Ovcharenko, M. Richter, M. Sauppe, S. Schorb, R. Treusch, D. Wolter, C. Bostedt and T. Moller, *Struct. Dyn.*, 2020, **7**, 034303.

85. N. N. Mude, R. N. Bukke, J. K. Saha, C. Avis and J. Jang, *Adv. Electronic Mater.*, 2019, **5**, 1900768.

86. E. Sowade, H. Kang, K. Y. Mitra, O. J. Weiß, J. Weber and R. R. Baumann, *J. Mater. Chem. C*, 2015, **3**, 11815-11826.

87. S. Sanchez, X. Hua, N. Phung, U. Steiner and A. Abate, *Adv. Energy Mater.*, 2018, **8**, 1702915.

88. S. Sanchez, N. Christoph, B. Grobety, N. Phung, U. Steiner, M. Saliba and A. Abate, *Adv. Energy Mater.*, 2018, **8**, 1802060.

89. Z. Ouyang, M. Yang, J. B. Whitaker, D. Li and M. F. A. M. v. Hest, *ACS Appl. Energy Mater.* , 2020, **3**, 3714−3720.

90. S. Sánchez, J. Jerónimo-Rendon, M. Saliba and A. Hagfeldt, *Mater. Today*, 2019, **35**, 9-15.

91. E. Ochoa-Martinez, M. Ochoa, R. D. Ortuso, P. Ferdowsi, R. Carron, A. N. Tiwari, U. Steiner and M. Saliba, *ACS Energy Lett.*, 2021, **6**, 2626−2634.

92. R. Román, I. Cañadas, J. Rodríguez, M. T. Hernández and M. González, *Sol. Energy*, 2008, **82**, 893-902.

93. A. Georgiadis, P. A. Bryant, M. Murray, P. Beharrell and J. L. Keddie, *Langmuir*, 2011, **27**, 2176-2180.

94. H. Guo, M. Peng, Z. Zhu and L. Sun, *Nanoscale*, 2013, **5**, 9040-9048.

95. X. Chen, Y. Chen, M. Yan and M. Qiu, *ACS Nano*, 2012, **6**, 2550-2557.

96. S. Sánchez, M. Vallés-Pelarda, J.-A. Alberola-Borràs, R. Vidal, J. J. Jerónimo-Rendón, M. Saliba, P. P. Boix and I. Mora-Seró, *Mater. Today* 2019, **31**, 1369-7021.

97. Y. Zhan, L. Xia, H. Yang, N. Zhou, G. Ma, T. Zhang, X. Huang, L. Xiong, C. Qin and W. Guangwu, *Carbon*, 2021, **175**, 101-111.

98. H. A. Albarqi, L. H. Wong, C. Schumann, F. Y. Sabei, T. Korzun, X. Li, M. N. Hansen, P. Dhagat, A. S. Moses, O. Taratula and O. Taratula, *ACS Nano*, 2019, **13**, 6383-6395.

99. T. Bayerl, M. Duhovic, P. Mitschang and D. Bhattacharyya, *Compos. Part A-Appl. S.*, 2014, **57**, 27-40.

100. D. De Masi, J. M. Asensio, P. F. Fazzini, L. M. Lacroix and B. Chaudret, *Angew. Chem. Int. Ed..*, 2020, **59**, 6187-6191.

101. C. Niether, S. Faure, A. Bordet, J. Deseure, M. Chatenet, J. Carrey, B. Chaudret and A. Rouet, *Nat. Energy*, 2018, **3**, 476-483.

102. W. Wang, C. Duong-Viet, Z. Xu, H. Ba, G. Tuci, G. Giambastiani, Y. Liu, T. Truong-Huu, J.-M. Nhut and C. Pham-Huu, *Catal. Today*, 2020, **357**, 214-220.

103. W. Wang, G. Tuci, C. Duong-Viet, Y. Liu, A. Rossin, L. Luconi, J.-M. Nhut, L. Nguyen-Dinh, C. Pham-Huu and G. Giambastiani, *ACS Catal.*, 2019, **9**, 7921-7935.

104. A. V. Ukhina, D. V. Dudina, A. G. Anisimov, V. I. Mali, N. V. Bulina, I. A. Bataev, I. N. Skovorodin and B. B. Bokhonov, *Ceram. Int.*, 2015, **41**, 12459-12463.

105. O. Guillon, J. Gonzalez-Julian, B. Dargatz, T. Kessel, G. Schierning, J. Räthel and M. Herrmann, *Adv. Eng. Mater.*, 2014, **16**, 830-849.

106. Y. Qin, J.-X. Liu, F. Li, X. Wei, H. Wu and G.-J. Zhang, *J. Adv. Ceram.*, 2019, **8**, 148-152.

107. Y. Orooji, E. Ghasali, M. Moradi, M. R. Derakhshandeh, M. Alizadeh, M. S. Asl and T. Ebadzadeh, *Ceram. Int.*, 2019, **45**, 16288-16296.

108. M. Yu, S. Grasso, R. McKinnon, T. Saunders and M. J. Reece, *Adv. Appl. Ceram.*, 2016, **116**, 24-60.

109. T. H. Im, J. H. Lee, H. S. Wang, S. H. Sung, Y. B. Kim, Y. Rho, C. P. Grigoropoulos, J. H. Park and K. J. Lee, *Mater. Today*, 2021, **51**, 1369-7021.

110. D.-H. Kim, J.-H. Cha, G. Shim, Y. H. Kim, J.-S. Jang, H. Shin, J. Ahn, S.-Y. Choi and I.-D. Kim, *Chem*, 2022, **8**, 1–20.

111. G. He, M. Yan, H. Gong, H. Fei and S. Wang, *Int. J. Extrem. Manuf.*, 2022, **4**, 032003.

112. Y. Oh, S.-N. Lee, H.-K. Kim and J. Kim, *J. Electrochem. Soc.*, 2012, **159**, H777-H781.

113. W.-H. Chung, S.-H. Park, S.-J. Joo and H.-S. Kim, *Nano Res.*, 2018, **11**, 2190-2203.

114. K. Wagner, A. J. Kell, Y. Martinez-Rubi, C. Paquet and B. H. Lessard, *Adv. Mater. Technol.-Us*, 2022, DOI: 10.1002/admt.202200037, 2200037.

115. Z. Huang, Y. Yao, Z. Pang, Y. Yuan, T. Li, K. He, X. Hu, J. Cheng, W. Yao, Y. Liu, A. Nie, S. Sharifi-Asl, M. Cheng, B. Song, K. Amine, J. Lu, T. Li, L. Hu and R. Shahbazian-Yassar, *Nat. Commun.*, 2020, **11**, 6373.

116. B. Wang, C. Wang, X. Yu, Y. Cao, L. Gao, C. Wu, Y. Yao, Z. Lin and Z. Zou, *Nat. Synth.*, 2022, **1**, 138-146.

117. G. A. Sotiriou, T. Sannomiya, A. Teleki, F. Krumeich, J. Voros and S. E. Pratsinis, *Adv. Funct. Mater.*, 2010, **20**, 4250-4257.

118. E. P. George, D. Raabe and R. O. Ritchie, *Nat. Rev. Mater.*, 2019, **4**, 515-534.

119. D. B. Miracle, *Nat. Common.*, 2019, **10**, 1805.

120. Q. Ding, Y. Zhang, X. Chen, X. Fu, D. Chen, S. Chen, L. Gu, F. Wei, H. Bei, Y. Gao, M. Wen, J. Li, Z. Zhang, T. Zhu, R. O. Ritchie and Q. Yu, *Nature*, 2019, **574**, 223-227.

121. H. Liu, L. Syama, L. Zhang, C. Lee, C. Liu, Z. Dai and Q. Yan, *SusMat.*, 2021, **1**, 482–505.

122. C. Oses, C. Toher and S. Curtarolo, *Nat. Rev. Mater.*, 2020, **5**, 295-309.

123. C. Zhao, Q. Wang, Z. Yao, J. Wang, B. Sánchez-Lengeling, F. Ding, X. Qi, Y. Lu, X. Bai, B. Li, H. Li, A. Aspuru-Guzik, X. Huang, C. Delmas, M. Wagemaker, L. Chen and Y.-S. Hu, *Science*, 2020, **370**, 708–711.

124. E. L. Septiani, S. Yamashita, K. L. A. Cao, T. Hirano, N. Okuda, H. Matsumoto, Y. Enokido and T. Ogi, *Ind. Eng. Chem. Res.*, 2022, DOI: 10.1021/acs.iecr.2c02837.

125. G. A. Sotiriou, A. M. Hirt, P. Y. Lozach, A. Teleki, F. Krumeich and S. E. Pratsinis, *Chem. Mater.*, 2011, **23**, 1985-1992.

126. N. Zhao and M. Gao, *Adv. Mater.*, 2009, **21**, 184-187.

127. Y. Zhang, B. Ouyang, J. Xu, S. Chen, R. S. Rawat and H. J. Fan, *Adv. Energy Mater.*, 2016, **6**, 1600221.

128. C. Yang, Y. Yao, S. He, H. Xie, E. Hitz and L. Hu, *Adv. Mater.*, 2017, **29**, 1702714.

129. L. Duan, L. Zhao, H. Cong, X. Zhang, W. Lu and C. Xue, *Small*, 2019, **15**, e1804347.

130. M. Hong, Q. Dong, H. Xie, B. C. Clifford, J. Qian, X. Wang, J. Luo and L. Hu, *ACS Energy Lett.*, 2021, **6**, 3753-3760.

131. G. Zhong, C. Wang, R. Wang, W. Ping, S. Xu, H. Qiao, M. Cui, X. Wang, Y. Zhou, D. J. Kline, M. R. Zachariah and L. Hu, *Energy Storage Mater.*, 2020, **30**, 385-391.

132. Y. Zhang, W. Luo, C. Wang, Y. Li, C. Chen, J. Song, J. Dai, E. M. Hitz, S. Xu, C. Yang, Y. Wang and L. Hu, *Proc. Natl. Acad. Sci. USA*, 2017, **114**, 3584–3589.

133. S. Xu, D. W. McOwen, C. Wang, L. Zhang, W. Luo, C. Chen, Y. Li, Y. Gong, J. Dai, Y. Kuang, C. Yang, T. R. Hamann, E. D. Wachsman and L. Hu, *Nano Lett.*, 2018, **18**, 3926-3933.

134. J. Y. Seok, S. Kim, I. Yang, J. H. Park, J. Lee, S. Kwon and K. Woo, *ACS Appl Mater Inter.*, 2021, **13**, 15205-15215.

135. W. Ping, C. Wang, R. Wang, Q. Dong, Z. Lin, A. H. Brozena, J. Dai, J. Luo and L. Hu, *Sci. Adv.*, 2020, **6**, eabc8641.

136. R. Pfenninger, M. Struzik, I. Garbayo, E. Stilp and J. L. M. Rupp, *Nat. Energy*, 2019, **4**, 475-483.

137. W. Li, G. Wu, C. M. Araújo, R. H. Scheicher, A. Blomqvist, R. Ahuja, Z. Xiong, Y. Feng and P. Chen, *Energ. Environ. Sci.*, 2010, **3**, 1524.

138. Y. Ye, L.-Y. Chou, Y. Liu, H. Wang, H. K. Lee, W. Huang, J. Wan, K. Liu, G. Zhou, Y. Yang, A. Yang, X. Xiao, X. Gao, D. T. Boyle, H. Chen, W. Zhang, S. C. Kim and Y. Cui, *Nat. Energy*, 2020, **5**, 786-793.

139. T. S. D. Le, Y. A. Lee, H. K. Nam, K. Y. Jang, D. Yang, B. Kim, K. Yim, S. W. Kim, H. Yoon and Y. J. Kim, *Adv. Funct. Mater.*, 2021, **32**, 2107768.

140. Y. Yuan, L. Jiang, X. Li, P. Zuo, C. Xu, M. Tian, X. Zhang, S. Wang, B. Lu, C. Shao, B. Zhao, J. Zhang, L. Qu and T. Cui, *Nat. Commun.*, 2020, **11**, 6185.

141. X. Shi, M. Liao, Y. Zuo, J. Wu, P. Zhai, J. Shen, Y. Yang, J. Wang, X. Xu, Q. Tong, B. Zhang, B. Wang, X. Sun, L. Zhang, Q. Pei, D. Jin and H. Peng, *Nature*, 2021, **591**, 240-245.

142. R. B. Ambade, H. Lee, K. Hyun Lee, H. Lee, G. Kumar Veerasubramani, Y.-B. Kim and T. Hee Han, *Chem. Eng. J.*, 2022, **436**, 135041.

143. L. J. Wang, M. F. El-Kady, S. Dubin, J. Y. Hwang, Y. Shao, K. Marsh, B. McVerry, M. D. Kowal, M. F. Mousavi and R. B. Kaner, *Adv. Energy Mater.*, 2015, **5**, 1500786.

144. H. Zhang, D. Yang, T. Ma, H. Lin and B. Jia, *Small Methods*, 2021, **5**, e2100225.

145. N. Rolston, W. J. Scheideler, A. C. Flick, J. P. Chen, H. Elmaraghi, A. Sleugh, O. Zhao, M. Woodhouse and R. H. Dauskardt, *Joule*, 2020, **4**, 2675–2692.

146. X. Xiao, C. Bao, Y. Fang, J. Dai, B. R. Ecker, C. Wang, Y. Lin, S. Tang, Y. Liu, Y. Deng, X. Zheng, Y. Gao, X. C. Zeng and J. Huang, *Adv. Mater.*, 2018, **30**, 1705176.

147. K. Khan, T. Liu, M. Arif, X. Yan, M. D. Hossain, F. Rehman, S. Zhou, J. Yang, C. Sun, S. H. Bae, J. Kim, K. Amine, X. Pan and Z. Luo, *Adv. Energy Mater.*, 2021, **11**, 2101619.

148. Z. Gong, R. Liu, H. Gong, G. Ye, J. Liu, J. Dong, J. Liao, M. Yan, J. Liu, K. Huang, L. Xing, J. Liang, Y. He and H. Fei, *ACS Catal.*, 2021, **11**, 12284-12292.

149. F. Hilt, M. Q. Hovish, C. J. Tassone, N. Rolston and R. H. Dauskardt, *Energy Environ. Sci.*, 2018, **11**, 2102--2113.

150. Y. Y. Kim, T. Y. Yang, R. Suhonen, A. Kemppainen, K. Hwang, N. J. Jeon and J. Seo, *Nat Commun*, 2020, **11**, 5146.

151. K. Bruening, B. Dou, J. Simonaitis, Y.-Y. Lin, M. F. A. M. van Hest and C. J. Tassone, *Joule*, 2018, **2**, 2464-2476.

152. A. Brunova, K. Vegso, V. Nadazdy, P. Nadazdy, R. Subair, M. Jergel, E. Majkova, P. Pandit, S. V. Roth, A. Krasnansky, A. Hinderhofer, F. Schreiber, J. Tian and P. Siffalovic, *Adv. Mater. Inter.*, 2021, **8**, 2100355.

153. A. Gunzler, E. Bermudez-Urena, L. A. Muscarella, M. Ochoa, E. Ochoa-Martinez, B. Ehrler, M. Saliba and U. Steiner, *ACS Appl. Mater. Inter.*, 2021, **13**, 6854-6863.

154. S. Sánchez, S. Cacovich, G. Vidon, J.-F. Guillemoles, F. Eickemeyer, S. M. Zakeeruddin, J. E. K. Schawe, J. F. Löffler, C. Cayron, P. Schouwink and M. Graetzel, *Energy Environ. Sci.*, 2022, **15**, 3862-3876.

155. B. Pang, X. Liu, T. Liu, T. Chen, X. Shen, W. Zhang, S. Wang, T. Liu, D. Liu, T. Ding, Z. L. Liao, Y. Li, C. Liang and T. Yao, *Energy Environ. Sci.*, 2022, **15**, 102-108.

156. Q. Liu and S. W. Chen, *Trends Chem.*, 2022, **4**, 918-934.

157. L. Li, P. Wang, Q. Shao and X. Huang, *Chem. Soc. Rev.*, 2020, **49**, 3072-3106.

158. H. Sun, X. Xu, Y. Song, W. Zhou and Z. Shao, *Adv. Funct. Mater.*, 2021, **31**, 2009779.

159. K. Hu, M. Wu, S. Hinokuma, T. Ohto, M. Wakisaka, J.-i. Fujita and Y. Ito, *J. Mater. Chem. A*, 2019, **7**, 2156-2164.

160. Z. L. Zhao, Q. Wang, X. Huang, Q. Feng, S. Gu, Z. Zhang, H. Xu, L. Zeng, M. Gu and H. Li, *Energ. Environ. Sci.*, 2020, **13**, 5143-5151.

161. J. Yu, B.-Q. Li, C.-X. Zhao and Q. Zhang, *Energ. Environ. Sci.*, 2020, **13**, 3253-3268.

162. H. Huang, D. Yu, F. Hu, S. C. Huang, J. Song, H. Y. Chen, L. L. Li and S. Peng, *Angew. Chem. Int. Ed.*, 2022, **61**, e202116068.

163. S. Liang, L. C. Zou, L. J. Zheng, F. Li, X. X. Wang, L. N. Song and J. J. Xu, *Adv. Energy Mater.*, 2022, **12**, 2103097.

164. N. Jiang, Z. Zhu, W. Xue, B. Y. Xia and B. You, *Adv. Mater.*, 2022, **34**, e2105852.

165. X. Wei, Y. Li, L. Chen and J. Shi, *Angew.Chem.Int. Ed.*, 2021, **60**, 3148-3155.

166. S. Verma, S. Lu and P. J. A. Kenis, *Nat. Energy*, 2019, **4**, 466-474.

167. S. Ding, H.-A. Chen, O. Mekasuwandumrong, M. J. Hülsey, X. Fu, Q. He, J. Panpranot, C.-M. Yang and N. Yan, *Appl. Catal. B-Environ.*, 2021, **281**, 119471.

168. S. Xiao, D. Zhang, D. Pan, W. Zhu, P. Liu, Y. Cai, G. Li and H. Li, *Nat. Commun.*, 2019, **10**, 1570.

169. S. Sun, X. Sha, J. Liang, G. Yang, X. Hu, Z. He, M. Liu, N. Zhou, X. Zhang and Y. Wei, *J. Hazard. Mater.*, 2021, **420**, 126580.

170. W. A. Algozeeb, P. E. Savas, D. X. Luong, W. Chen, C. Kittrell, M. Bhat, R. Shahsavari and J. M. Tour, *ACS Nano*, 2020, **14**, 15595−15604.

171. M. Naguib, M. Kurtoglu, V. Presser, J. Lu, J. j. Niu, M. Heon, L. Hultman, Y. Gogotsi and M. W. Barsoum, *Adv. Mater.*, 2011, **23**, 4248-4253.

172. B. C. Gibb, *Nat. Chem.*, 2019, **11**, 394-395.

173. R. Geyer, J. R. Jambeck and K. L. Law, *Sci. Adv.*, 2017, **3**, e1700782.

174. M. Jiao, Q. Zhang, C. Ye, Z. Liu, X. Zhong, J. Wang, C. Li, L. Dai, G. Zhou and H. M. Cheng, *Proc. Natl. Acad. Sci. USA*, 2022, **119**, e2202202119.

175. S. Dong, Y. Song, K. Ye, J. Yan, G. Wang, K. Zhu and D. Cao, *EcoMat.*, 2022, DOI: 10.1002/eom2.12212, e12212.

176. X. Zhang, L. Li, E. Fan, Q. Xue, Y. Bian, F. Wu and R. Chen, *Chem. Soc. Rev.*, 2018, **47**, 7239-7302.

177. E. Fan, L. Li, Z. Wang, J. Lin, Y. Huang, Y. Yao, R. Chen and F. Wu, *Chem. Rev.*, 2020, **120**, 7020-7063.

178. Q. Dong, T. Li, Y. Yao, X. Wang, S. He, J. Li, J. Luo, H. Zhang, Y. Pei, C. Zheng, M. Hong, H. Qiao, J. Gao, D. Wang, B. Yang and L. Hu, *Joule*, 2020, **4**, 2374-2386.

179. Y. Chen, G. C. Egan, J. Wan, S. Zhu, R. J. Jacob, W. Zhou, J. Dai, Y. Wang, V. A. Danner, Y. Yao, K. Fu, Y. Wang, W. Bao, T. Li, M. R. Zachariah and L. Hu, *Nat. Commun.*, 2016, **7**, 12332.

180. C. Liu, Y. Shen, J. Zhang, G. Li, X. Zheng, X. Han, L. Xu, S. Zhu, Y. Chen, Y. Deng and W. Hu, *Adv. Energy Mater.* , 2022, **12**, 2103505.

181. C. Liu, W. Zhou, J. Zhang, Z. Chen, S. Liu, Y. Zhang, J. Yang, L. Xu, W. Hu, Y. Chen and Y. Deng, *Adv. Energy Mater.*, 2020, **10**, 2001397.

182. B. Deng, Z. Wang, W. Chen, J. T. Li, D. X. Luong, R. A. Carter, G. Gao, B. I. Yakobson, Y. Zhao and J. M. Tour, *Nat. Commun.*, 2022, **13**.

183. S. Liu, P. Wang, C. Liu, Y. Deng, S. Dou, Y. Liu, J. Xu, Y. Wang, W. Liu, W. Hu, Y. Huang and Y. Chen, *Small*, 2020, **16**, e2002856.

184. W. Chen, Z. Wang, K. V. Bets, D. X. Luong, M. Ren, M. G. Stanford, E. A. McHugh, W. A. Algozeeb, H. Guo, G. Gao, B. Deng, J. Chen, J. T. Li, W. T. Carsten, B. I. Yakobson and J. M. Tour, *ACS Nano*, 2021, **15**, 1282-1290.

185. D. X. Luong, K. V. Bets, W. A. Algozeeb, M. G. Stanford, C. Kittrell, W. Chen, R. V. Salvatierra, M. Ren, E. A. McHugh, P. A. Advincula, Z. Wang, M. Bhatt, H. Guo, V. Mancevski, R. Shahsavari, B. I. Yakobson and J. M. Tour, *Nature*, 2020, **577**, 647-651.

186. M. Guo, Q. Dong, H. Xie, C. Wang, Y. Zhao, X. Wang, W. Zhong, Z. Li, R. Wang, Y. Wang, L. Hao, S. He, G. Chen, W. Xiong, J.-C. Zhao and L. Hu, *Matter*, 2021, DOI: 10.1016/j.matt.2021.11.008.

187. J. Xie, J. Yan, D. Zhu and G. He, *Adv. Funct. Mater.s*, 2021, **32**, 2108802.

188. Q. Li, Q. Wang, L. Li, L. Yang, Y. Wang, X. Wang and H. T. Fang, *Adv. Energy Mater.*, 2020, **10**, 2000470.

189. S. Huang, X. Du, X. Li, M. Ma and L. Xiong, *Adv. Funct. Mater.*, 2021, **31**, 2104531.

190. F. Zhang, E. Alhajji, Y. Lei, N. Kurra and H. N. Alshareef, *Adv. Energy Mater.* , 2018, **8**, 1800353.

191. W. Zhang, R. Li, H. Zheng, J. Bao, Y. Tang and K. Zhou, *Adv. Funct. Mater.*, 2021, **31**, 2009057.

192.   Alexey Y. Zhizhchenko, P. Tonkaev, D. Gets, A. Larin, D. Zuev, S. Starikov, E. V. Pustovalov, A. M. Zakharenko, S. A. Kulinich, S. Juodkazis, A. A. Kuchmizhak and S. V. Makarov, *Small*, 2020, **16**, e2000410.

193.   H. Fei, J. Dong, C. Wan, Z. Zhao, X. Xu, Z. Lin, Y. Wang, H. Liu, K. Zang, J. Luo, S. Zhao, W. Hu, W. Yan, I. Shakir, Y. Huang and X. Duan, *Adv. Mater.*, 2018, **30**, e1802146.

194.   M. Kheradmandfard, H. Minouei, N. Tsvetkov, A. K. Vayghan, S. F. Kashani-Bozorg, G. Kim, S. I. Hong and D.-E. Kim, *Mater. Chem. Phys.*, 2021, **262**, 124265.

195.   Y. Tian, S. Sarwar, Y. Zheng, S. Wang, Q. Guo, J. Luo and X. Zhang, *J. Solid State Electr.*, 2020, **24**, 809-819.

196.   H. Jiang, W. Liu, X. Zhang and J. Qiao, *Glob. Chall.*, 2020, **4**, 1900074.

197.   G. Xu, H. Jiang, M. Stapelberg, J. Zhou, M. Liu, Q. J. Li, Y. Cao, R. Gao, M. Cai, J. Qiao, M. S. Galanek, W. Fan, W. Xue, B. Marelli, M. Zhu and J. Li, *Environ. Sci. Technol.*, 2021, **55**, 6239-6247.

198.   R. Liu, Y. Zhang, Z. Ning and Y. Xu, *Angew. Chem. Int. Ed. Engl.*, 2017, **56**, 15677-15682.

199.   K. Fujiwara and S. E. Pratsinis, *Appl. Catal. B-Environ.*, 2018, **266**, 127-134.

200.   C. Abram, J. Shan, X. Yang, C. Yan, D. Steingart and Y. Ju, *ACS Appl. Energy Mater.*, 2019, **2**, 1319-1329.

201.   K. A. Michalow-Mauke, Y. Lu, K. Kowalski, T. Graule, M. Nachtegaal, O. Kröcher and D. Ferri, *ACS Catal.*, 2015, **5**, 5657-5672.

202.   H. Li, S. Pokhrel, M. Schowalter, A. Rosenauer, J. Kiefer and L. Madler, *Combust Flame*, 2020, **215**, 389-400.

203.   Z. Ma, H. Tian, L. Cong, Q. Wu, M. Yue and S. Sun, *Angew. Chem. Int. Ed.*, 2019, **58**, 14509-14512.

204.   Y. Zhang, B. Ouyang, K. Xu, X. Xia, Z. Zhang, R. S. Rawat and H. J. Fan, *Small*, 2018, **14**, e1800340.

205.   Q. Liu, B. Lu, F. Nichols, J. Ko, R. Mercado, F. Bridges and S. Chen, *SusMat.*, 2022, **2**, 335-346.

206.   B. D. Sosnowchik and L. Lin, *Appl. Phys. Lett.*, 2006, **89**, 193112.

207.   C. Wu, F. Li, W. Chen, C. P. Veeramalai, P. C. Ooi and T. Guo, *Sci Rep*, 2015, **5**, 9034.

208.   X. Wang, Z. Huang, Y. Yao, H. Qiao, G. Zhong, Y. Pei, C. Zheng, D. Kline, Q. Xia, Z. Lin, J. Dai, M. R. Zachariah, B. Yang, R. Shahbazian-Yassar and L. Hu, *Mater. Today*, 2020, **35**, 106-114.

209.   M. Jiao, Y. Yao, G. Pastel, T. Li, Z. Liang, H. Xie, W. Kong, B. Liu, J. Song and L. Hu, *Nanoscale*, 2019, **11**, 6174-6181.

210.   Y. Cheng, G. Cui, C. Liu, Z. Liu, L. Yan, B. Liu, H. Yuan, P. Shi, J. Jiang, K. Huang, K. Wang, S. Cheng, J. Li, P. Gao, X. Zhang, Y. Qi and Z. Liu, *Adv. Funct. Mater.*, 2021, DOI: 10.1002/adfm.202103493.

211.   B. Shi, Y. Shang, P. Zhang, A. P. Cuadros, J. Qu, B. Sun, B. Gu, T.-W. Chou and K. Fu, *Matter*, 2020, **2**, 1594-1604.

212.   Y. Wang, Y. Wang, P. Zhang, F. Liu and S. Luo, *Small*, 2018, **14**, 1802350.

213.   Y. Liu, P. Li, F. Wang, W. Fang, Z. Xu, W. Gao and C. Gao, *Carbon*, 2019, **155**, 462-468.

214.   F. Bisconti, A. Giuri, R. Suhonen, T. M. Kraft, M. Ylikunnari, V. Holappa, R. Po', P. Biagini, A. Savoini, G. Marra, S. Colella and A. Rizzo, *Cell Rep. Phys. Sci.*, 2021, **2**, 100639.

215.   N. Rolston, A. Sleugh, J. P. Chen, O. Zhao, T. W. Colburn, A. C. Flick and R. H. Dauskardt, *Front. Energy Res.*, 2021, **9**, 684082.

216.   J. H. Martin, B. D. Yahata, J. M. Hundley, J. A. Mayer, T. A. Schaedler and T. M. Pollock, *Nature*, 2017, **549**, 365-369.

217.   X. Wang, Y. Zhao, G. Chen, X. Zhao, C. Liu, S. Sridar, L. F. L. Pizano, S. Li, A. H. Brozena, M. Guo, H. Zhang, Y. Wang, W. Xiong and L. Hu, *Nat. Commun.*, 2022, **13**, 6724.

218.   T. Zhao, A. Elzatahry, X. Li and D. Zhao, *Nat. Rev. Mater.*, 2019, **4**, 775-791.

219.   L. Huang, H. Lin, C. Y. Zheng, E. J. Kluender, R. Golnabi, B. Shen and C. A. Mirkin, *J. Am. Chem. Soc.*, 2020, **142**, 4570−4575.

220.   J. Wang, J. Wan, N. Yang, Q. Li and D. Wang, *Nat. Rev. Chem.*, 2020, **4**, 159-168.

221.   X. Cui, W. Li, P. Ryabchuk, K. Junge and M. Beller, *Nat. Catal.*, 2018, **1**, 385-397.

222.   H. Xie, Y. Liu, N. Li, B. Li, D. J. Kline, Y. Yao, M. R. Zachariah, G. Wang, D. Su, C. Wang and L. Hu, *Nano Energy*, 2021, **80**, 105536.

223.   Y. Chen, Y. Li, Y. Wang, K. Fu, V. A. Danner, J. Dai, S. D. Lacey, Y. Yao and L. Hu, *Nano Lett.*, 2016, **16**, 5553-5558.

224.   Y. Zhou, Q. Bao, B. Varghese, L. A. Tang, C. K. Tan, C. H. Sow and K. P. Loh, *Adv. Mater.*, 2010, **22**, 67-71.

225.   D. Wei, J. I. Mitchell, C. Tansarawiput, W. Nam, M. Qi, P. D. Ye and X. Xu, *Carbon*, 2013, **53**, 374-379.

226.   S. Moussa, G. Atkinson, M. SamyEl-Shall, A. Shehata, K. M. AbouZeid and M. B. Mohamed, *J. Mater. Chem.*, 2011, **21**, 9608.

227.   C. Huang, C. Zhang, S. Xiao, Y. Wang, Y. Fan, Y. Liu, N. Zhang, G. Qu, H. Ji, J. Han, L. Ge, Y. Kivshar and Q. Song, *Science*, 2020, **376**, 1018–1021

228.   R. Y. Gengler, D. S. Badali, D. Zhang, K. Dimos, K. Spyrou, D. Gournis and R. J. Miller, *Nat. Commun.*, 2013, **4**, 2560.

229.   R. Liu, Y. Zhang, Z. Ning and Y. Xu, *Angew. Chem. Int. Ed.*, 2017, **56**, 15677-15682.

230.   K. Yan, X. Sun, S. Ying, W. Cheng, Y. Deng, Z. Ma, Y. Zhao, X. Wang, L. Pan and Y. Shi, *Sci. Rep.*, 2020, **10**, 6227.

231.   Z. Hu, Y. Lv, C. Zhao, Q. Feng, Z. Feng, K. Dang, X. Tian, Y. Zhang, J. Ning, H. Zhou, X. Kang, J. Zhang and Y. Hao, *IEEE Electr. Device L.*, 2020, **41**, 441-444.

232.   K. Jiang, L. Zhu, Z. Wang, K. Liu, H. Li, J. Hu, H. Pan, J. Fu, N. Zhang, X. Qiu and M. Liu, *Appl. Surf. Sci.*, 2020, **508**, 145173.

233.   G. B. Yadhukulakrishnan, S. Karumuri, A. Rahman, R. P. Singh, A. Kaan Kalkan and S. P. Harimkar, *Ceram. Int.*, 2013, **39**, 6637-6646.

234.   A. Bellosi, F. d. r. Monteverde and D. Sciti, *Int. J. Appl. Ceram. Technol.*, 2006, **3** 32–40.

235.   R. Koirala, S. E. Pratsinis and A. Baiker, *Chem. Soc. Rev.*, 2016, **45**, 3053-3068.

236.   H. Li, C. D. Rosebrock, N. Riefler, T. Wriedt and L. Mädler, *P. Combust. Inst.*, 2017, **36**, 1011-1018.

237.   Y. Wang, C. A. Mirkin and S.-J. Park, *ACS Nano*, 2009, **3**, 1049–1056

238.   J. Meng, W. Nie, K. Zhang, F. Xu, X. Ding, S. Wang and Y. Qiu, *ACS Appl. Mater. Inter.*, 2018, **10**, 13652-13659.

239.   C. Arpagaus, G. Oberbossel and P. Rudolf von Rohr, *Plasma Process. Polym.*, 2018, **15**, 1800133.

240.   T. Sun, Y. Wang, Y. Long, Q. Li and G. Fan, *Fuel*, 2022, **309**, 122203.

241. A. Dey, P. Ghosh, G. Chandrabose, L. A. O. Damptey, N. Kuganathan, S. Sainio, D. Nordlund, V. Selvaraj, A. Chroneos, N. St J. Braithwaite and S. Krishnamurthy, *Nano Select*, 2021, **3**, 627-642.

242. A. H. Phakatkar, M. T. Saray, M. G. Rasul, L. V. Sorokina, T. G. Ritter, T. Shokuhfar and R. Shahbazian-Yassar, *Langmuir*, 2021, **37**, 9059-9068.

243. L. Li, J. Zhang, Y. Wang, F. U. Zaman, Y. Zhang, L. Hou and C. Yuan, *InfoMat.*, 2021, **3**, 1393–1421.

244. L. Zhao, Z. Liu, D. Chen, F. Liu, Z. Yang, X. Li, H. Yu, H. Liu and W. Zhou, *Nano-Micro Lett.*, 2021, **13**, 49.

245. R. Jiang, Y. Da, X. Han, Y. Chen, Y. Deng and W. Hu, *Cell Rep. Phys. Sci.*, 2021, **2**, 100302.

246. Y. Yao, Z. Huang, T. Li, H. Wang, Y. Liu, H. S. Stein, Y. Mao, J. Gao, M. Jiao, Q. Dong, J. Dai, P. Xie, H. Xie, S. D. Lacey, I. Takeuchi, J. M. Gregoire, R. Jiang, C. Wang, A. D. Taylor, R. Shahbazian-Yassar and L. Hu, *Proc. Natl. Acad. Sci. USA*, 2020, **117**, 6316-6322.

247. Y. Yao, Q. Dong, A. Brozena, J. Luo, J. Miao, M. Chi, C. Wang, I. G. Kevrekidis, Z. J. Ren, J. Greeley, G. Wang, A. Anapolsky and L. Hu, *Science*, 2022, **376**, eabn3103.

248. J. Zhang, D. Zhu, J. Yan and C. A. Wang, *Nat. Commun.*, 2021, **12**, 6665.

249. Q. Xu, Q. Kong, Z. Liu, X. Wang, R. Liu, J. Zhang, L. Yue, Y. Duan and G. Cui, *ACS Sustain. Chem. Eng.*, 2013, **2**, 194-199.

250. W. Zhou, Y. Li, S. Xin and J. B. Goodenough, *ACS Cent. Sci.*, 2017, **3**, 52-57.

251. V. Sharma, M. Aman and S. Omar, *ACS Applied Nano Mater.*, 2022, **5**, 15651-15664.

252. Y. W. Han, H. S. Lee and D. K. Moon, *ACS Appl Mater Interfaces*, 2021, **13**, 19085-19098.

253. Y. Liu, L. J. Wang, H. Zhang, H. Y. Yuan, Q. Zhang, L. Gu, H. F. Wang, P. Hu, P. F. Liu, Z. Jiang and H. G. Yang, *Angew. Chem. In. Ed.*, 2021, **60**, 23027-23027.

254. J. Ren, S. Ouyang, H. Xu, X. Meng, T. Wang, D. Wang and J. Ye, *Adv. Energy Mater.*, 2017, **7**, 201770022.

255. D. Huang, N. He, Q. Zhu, C. Chu, S. Weon, K. Rigby, X. Zhou, L. Xu, J. Niu, E. Stavitski and J.-H. Kim, *ACS Catalysis*, 2021, **11**, 5586-5592.

256. J. Li, H. Duan and K. Pu, *Adv. Mater.*, 2019, **31**, e1901607.

257. A. J. Bandodkar, P. Gutruf, J. Choi, K. Lee, Y. Sekine, J. T. Reeder, W. J. Jeang, A. J. Aranyosi, S. P. Lee, J. B. Model, R. Ghaffari, C.-J. Su, J. P. Leshock, T. Ray, A. Verrillo, K. Thomas, V. Krishnamurthi, S. Han, J. Kim, S. Krishnan, T. Hang and J. A. Rogers, *Sci. Adv.*, 2019, **5**, eaav3294.

258. A. W. Mahoney and J. J. Abbott, *IEEE Robot.*, 2014, **30**, 411-420.